Journal of Hydrology 628 (2024) 130461

Contents lists available at ScienceDirect

Journal of Hydrology

journal homepage: www.elsevier.com/locate/jhydrol

Research papers

Mapping the vulnerability of groundwater to saltwater intrusion from estuarine rivers under sea level rise

Irene Setiawan[a,b,*], Leanne K. Morgan[b,*], Crile Doscher[a,b]

[a] Faculty of Environment, Society and Design, Lincoln University, PO Box 85084, Lincoln 7647, New Zealand
[b] Waterways Centre for Freshwater Management, School of Earth and Environment, University of Canterbury, Private Bag 4800, New Zealand

ARTICLE INFO

This manuscript was handled by N Basu, Editor-in-Chief, with the assistance of Magdalena Bieroza, Associate Editor

Keywords:
Analytic solutions
GALDIT–SUSI
Estuary
Climate change
Salinization
GIS

ABSTRACT

Surface water bodies connected to the ocean such as estuarine rivers can act as pathways for saltwater intrusion (SI, i.e., the displacement of fresh groundwater by saltwater in an aquifer) far inland of the coast, presenting one of the earliest risks associated with relative sea level rise (SLR). However, SI vulnerability mapping approaches have largely focused on SI from the coast and do not consider estuarine surface water bodies, except for GALDIT–SUSI (Kazakis et al., 2019); a weighted indexing approach designed for regional-scale mapping applications using a Geographic Information Systems (GIS) framework. However, GALDIT-SUSI is subjective in ranking the importance of factors that can contribute to SI and combining these into a vulnerability index. A less subjective approach to assessing SI vulnerability than weighted indexing methods involves the use of physically-based analytic solutions such as Strack (1976), but these have not been applied in a GIS framework or along estuaries and rivers previously. Here, these analytic solutions, surface water salinity, and surface water-groundwater freshwater head gradients are used in the development of a new SI vulnerability tier system. This new approach was applied in the low-lying coastal city of Ōtautahi Christchurch, Aotearoa New Zealand, along 70 km of coastal, estuary, and river margins under current sea level and SLR using GIS, then compared to GALDIT–SUSI. The main advantage of the SI vulnerability tiers method is that it considers surface water behaviour, e.g., increased saltwater encroachment up rivers under SLR, which exposed new areas of the aquifer to saltwater and increased SI vulnerability upstream. In contrast, GALDIT-SUSI does not consider surface water conditions and accounts for topography and groundwater level as the main SI vulnerability drivers in this application. The SI vulnerability tiers proposed here are more theoretically robust than GALDIT-SUSI and provide a physically-based, large-scale, relatively low-budget and rapid screening tool to highlight areas most vulnerable to SI under current and future conditions for further monitoring and management; a gap of national and international relevance.

1. Introduction

The protection and sustainable management of fresh groundwater resources are imperative to meet current and future freshwater needs under increasing anthropogenic and climatic pressures. Saltwater intrusion (SI), i.e., the displacement of fresh groundwater by saltwater in an aquifer (Jiao & Post, 2019), is a worldwide environmental issue that can lead to the contamination or loss of life–sustaining freshwater supply (Werner et al., 2013). Even though research has largely focused on SI occurring from the coast (e.g., Beebe et al., 2016; Befus et al., 2020; Ketabchi et al., 2016; Werner et al., 2013), surface water bodies hydrologically connected to the ocean such as canals, ditches, estuaries, and rivers can act as crucial conduits that facilitate the movement of saltwater upstream of the coast causing shallow aquifer salinization far inland (Bhattachan et al., 2018; Hingst et al., 2022; Parker et al., 1955; Tully et al., 2019). While SI occurring from the coast salinizes deep groundwater first and can cause saltwater upconing into deep water supply wells (Werner et al., 2013), SI from surface water bodies can first result in shallow groundwater salinization (Lenkopane et al., 2009; Werner and Lockington, 2006).

SI into shallow groundwater can cause stress or death to salt–intolerant species (Kirwan & Gedan, 2019; Mazhar et al., 2022), impact groundwater–dependent ecosystems (Eamus et al., 2016), salinize soils (Prathapar et al., 1992), and cause eutrophication in surface water

* Corresponding authors.
E-mail addresses: irene.setiawan@lincolnuni.ac.nz (I. Setiawan), leanne.morgan@canterbury.ac.nz (L.K. Morgan), crile.doscher@lincoln.ac.nz (C. Doscher).

https://doi.org/10.1016/j.jhydrol.2023.130461
Received 30 May 2023; Received in revised form 14 October 2023; Accepted 29 October 2023
Available online 14 November 2023

bodies (Weissman & Tully, 2020). In urban areas, shallow groundwater salinization can prematurely damage co–existing infrastructure such as underground pipes, building and road foundations (Luo et al., 2015) and impact wastewater treatment plant operations (Osman et al., 2017). SI into the shallow aquifer can also lead to deep groundwater salinization under sustained downward hydraulic gradients (e.g., Onodera et al., 2008). The cascading consequences of SI can significantly influence community health, well–being, and livelihoods (Dasgupta et al., 2014; Moorhead & Brinson, 1995; Shammi et al., 2019).

Factors that influence SI from surface water bodies include the permeability and heterogeneity of surface water bed and the adjacent aquifer, the hydraulic gradient that drives surface water-groundwater flow, and surface water salinity (Lenkopane et al., 2009; Shalem et al., 2015; Webster et al., 1996). Land subsidence and climate change impacts including sea level rise (SLR), increased frequency and intensity of storms and tides, reduced groundwater recharge, and reduced surface water flows, combined with anthropogenic stresses such as dam construction, increased groundwater extraction, surface water extraction, and artificial land drainage, are likely to exacerbate SI from surface water bodies (Bhattachan et al., 2018; Lorenz, 2014; Peters et al., 2022; Tully et al., 2019).

This study focuses on SI from estuarine rivers (also termed riparian SI; Setiawan et al., 2023) under SLR. Transitional environments such as estuarine water bodies are one of the first ecosystems to experience the impacts of SLR including increased saltwater encroachment (Costa et al., 2023), preceding tidal inundation at the land surface (Bhattachan et al., 2019; Tully et al., 2019). Saltwater encroachment occurs when saltwater from oceans moves upstream into rivers (e.g., Shalem et al., 2019). SLR increases river salinity and causes saltwater within estuarine rivers to impinge further upstream, causing previously fresh reaches to become brackish (Herbert et al., 2015). The understanding of estuarine river behaviour under SLR (e.g., salinity and water level) is therefore important to determine riparian SI vulnerability under SLR.

Increased saltwater encroachment into rivers exposes new parts of the aquifer to saltwater and increases the risk of groundwater salinization (Tully et al., 2019). As river salinity increases, the saltwater re–circulation zone in the aquifer beneath the riverbed can expand because of higher buoyancy forces (Lenkopane et al., 2009). The increase in river level and salinity due to SLR (e.g., Bhuiyan & Dutta, 2012) can cause the adjacent groundwater to rise and extend the saltwater wedge further inland within the aquifer, depending on inland boundary conditions (Bosserelle et al., 2022; Werner & Simmons, 2009; Werner et al., 2012).

In response to SLR, water table levels can rise (i.e., fixed flux boundary condition) if there is enough unsaturated space, or stay constant (i.e., fixed head boundary condition), which can occur due to land drainage and pumping (Bosserelle et al., 2022; Werner & Simmons, 2009). The rise in groundwater levels means that hydraulic gradients are maintained and fresh groundwater discharge is persistent despite SLR, which counteracts the force of saltwater intruding inland and minimizes salinization (Werner & Simmons, 2009). Many coastal cities worldwide were built on low–lying swamplands where groundwater levels were near or at the land surface, made possible by extensive drainage (Barlow & Reichard, 2010; Bosserelle et al., 2022; Parsons et al., 2021). Damaged subsurface pipe infrastructure (e.g., due to ageing or earthquake damage) can also act as groundwater drains (Liu et al., 2018). As these drainage systems keep groundwater at a constant level, they can cause the worst–case SI due to the reduction in fresh groundwater discharge and hydraulic gradients under SLR (Lu et al., 2013; Werner & Simmons, 2009).

To the authors' knowledge, GALDIT–SUSI is the only existing method that aims to determine large–scale aquifer vulnerability to SI while considering surface water bodies as sources of salinity (Kazakis et al., 2019). In general, this approach combines hydrogeological factors with different weightings based on their perceived importance in causing SI into one vulnerability index. Therefore, this method employs a high degree of subjectivity (Morgan et al., 2013; Werner et al., 2012). SI vulnerability at the coast under SLR has been assessed using the physically-based analytic solutions of Strack (1976) (Morgan & Werner, 2015; Werner et al., 2012), which is less subjective than weighted indexing approaches. Earlier studies applied the analytic solutions in coastal settings to a representative cross–section per aquifer (Morgan & Werner, 2015; Morgan et al., 2013; Werner et al., 2012) and multiple points along the coast (Wriedt & Bouraoui, 2009). However, these analytic solutions have not been previously applied in riparian or estuarine settings, and only one study mapped analytic solutions results along the coast (Wriedt & Bouraoui, 2009).

Here, the analytic solutions were applied along coastal, estuary, and river margins using a Geographic Information System (GIS) under current sea level and future SLR scenarios, for the first time. GIS–based vulnerability mapping allows SLR scenarios to be evaluated based on local topography (Luoma et al., 2017; Setiawan, 2018), a technical advantage that other modelling methods may lack. Although numerical modelling offers the most accurate representation of aquifer vulnerability to stressors, it is a more resource-intensive approach compared to SI vulnerability mapping using GIS (Klassen & Allen, 2017). Coupled groundwater-surface water models required to model riparian SI (e.g., Dibaj et al., 2021) on a regional scale or wider can be complex and data-intensive to build and calibrate. In lieu of this resource availability, this study proposes a simpler yet physically based approach to undertake a large-scale approximation of riparian SI vulnerability, which can help target areas for further monitoring. This approach is applicable to coastal areas with surface water bodies that experience saltwater encroachment (e.g., rivers, canals, drains, and ditches) and are in hydraulic connection with the adjacent groundwater. In addition, this approach considers lateral SI through surface water banks and beds and does not consider downward saltwater intrusion driven by episodic coastal floods (Cantelon et al., 2022) or where surface water overtops riverbanks (e.g., Liu et al., 2022; Shen et al., 2015; Xin et al., 2022). Paleoseawater as a source of shallow groundwater salinity (e.g., Worland et al., 2015) is not considered in the current research.

Riparian SI is an increasing concern under climate change. However, to the authors' knowledge, no study has attempted to map its vulnerability under SLR using physically-based methods. This paper expands on the current literature by aiming to: (i) apply the physically-based analytic solutions of Strack (1976) along coastal margins in a GIS environment, and extend the application to river and estuary margins to assess SI vulnerability from these surface water bodies under current and future SLR, (ii) develop and map SI vulnerability tiers based on the analytic solutions in a manner that is easy to understand and communicate, which can be useful for managers and decision–makers, (iii) compare the analytic solutions to the GALDIT–SUSI vulnerability indexing approach of Kazakis et al. (2019) under current sea level and future SLR. GALDIT-SUSI was applied as a comparative GIS-based approach and not as a validation. The SI vulnerability tiers proposed here can provide a physically–based, large–scale, relatively low–budget and rapid screening tool to highlight areas most vulnerable to SI under current and future conditions for further monitoring and management, a gap of national (in Aotearoa New Zealand) and international relevance (Controller and Auditor-General, 2020; Werner et al., 2013).

2. Materials and methods

2.1. Study area

Ōtautahi Christchurch (forthwith Ōtautahi) is a coastal city on the east coast of Te Waipounamu the South Island of Aotearoa New Zealand, where Ngāi Tāhu and Ngāi Tūāhuriri exercise mana whenua (indigenous sovereignty) (Hobbs et al., 2022). Located behind sand dunes, estuaries, and lagoons, the relatively flat and low–lying city was predominantly built on swampland drained by European settlers from the late 1800 s (Wilson, 1989). The city was able to be built owing to the extensive artificial drainage network of subsoil drains, utility waterways, and stormwater pipelines that reduce groundwater levels (Christchurch City Council, 2003). The climate in Ōtautahi is temperate with a mean annual rainfall of 618 mm and a median annual temperature of 11–13 °C from 1981 to 2010 (Macara, 2016). In June 2022, Ōtautahi had an estimated population of 389,300 people (the second–largest urban area population nationally) (Stats NZ, 2022), who rely entirely on groundwater for their water supply (Christchurch City Council, 2021).

The coastal aquifer system in Ōtautahi is multi–layered and extends offshore, comprising at least four highly productive gravel aquifers deposited during glacial periods alternating with confining layers of marine sediments deposited during interglacial periods (Begg et al., 2015; Brown, 2001). The dominant source of aquifer recharge is river seepage from the north of the city as well as rainfall infiltration (Stewart, 2012). Inland from Ōtautahi, groundwater is used to support large–scale farming industries (Brown, 2001). The coastal aquifer system is an upward flow or discharge zone, where the deep confined aquifers have greater pressure than the shallow water table aquifer and groundwater emerges as springs (Cox et al., 2021; Stewart et al., 2018).

The present study investigates the SI vulnerability of the shallow unconfined aquifer named the Christchurch Formation, which is made predominantly of sand and silt with shells, minor peat and thin sandy gravel lenses deposited since about 8,000 BCE (Begg et al., 2015). The Christchurch Formation is approximately 35 m thick near the coast, gradually thinning inland, and ends about 10 km inland from the coast (Begg et al., 2015). The water table aquifer is hydrologically connected to the rivers, where tidal fluctuations propagate from the ocean into the estuary, rivers, and shallow groundwater up to a few kilometres inland (Bosserelle et al., 2023). A groundwater salinity survey of the Christchurch Formation observed brackish groundwater along the estuarine reach of the Ōtākaro River and the sand dune spit between Pegasus Bay and the Ihutai estuary (Setiawan et al., 2022b) (Fig. 1).

The surface water bodies focused on in this study are the Ōtākaro Avon River (forthwith Ōtākaro) and Ōpāwaho Heathcote River (forthwith Ōpāwaho). These were traditionally important mahinga kai (food–gathering place) for mana whenua (Christchurch City Council, 2016; Ōpāwaho Heathcote River Network, 2021). Both the Ōtākaro and Ōpāwaho are high–order rivers that originate from spring–fed headwaters and flow across the city while receiving stormwater inputs, and into the Ihutai Avon–Heathcote estuary (forthwith Ihutai). The two rivers have estuarine reaches and saltwater encroaches a few kilometres upstream depending on river flow and tide conditions (Orchard & Measures, 2016; Orchard & Measures, 2017). Tidally fluctuating shallow groundwater salinity has been observed adjacent to the estuarine reach of the Ōtākaro (Setiawan et al., 2023). The Ōpāwaho has a tidal barrage that is designed to fully prevent saltwater from flowing upstream, however, this has been reported to leak and saltwater has been observed to flow upstream of the barrage (Orchard & Measures, 2016). Land subsidence trends of 41 mm year^{-1} in the Ōpāwaho River mouth area and 39 mm year^{-1} in the Ōtākaro River mouth area were

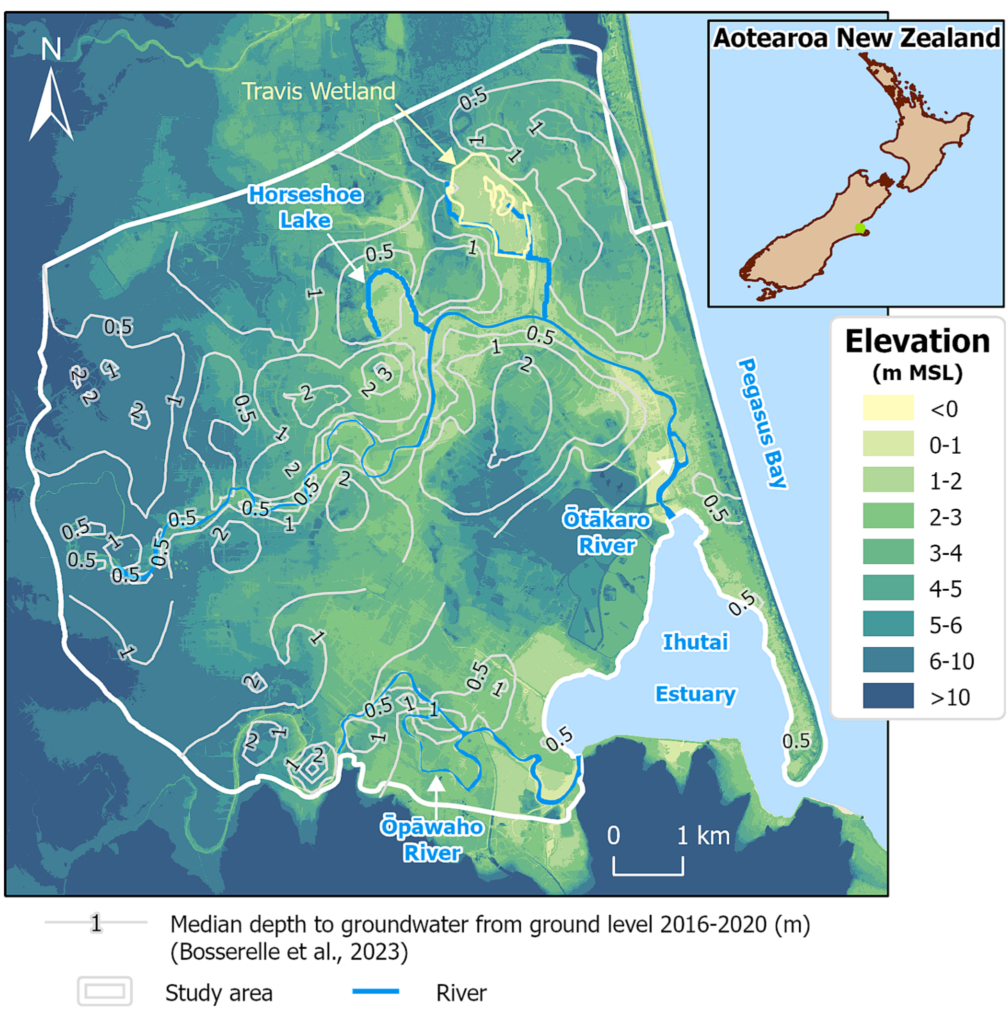

Fig. 1. Study area map with elevation (converted to mean sea level or MSL from Land Information New Zealand, 2021), contours of median depth to groundwater from ground level 2016–2020 (Bosserelle et al., 2023), rivers (Land Information New Zealand, 2011a, b) (only a selection are displayed here), Travis Wetland outline (Manaaki Whenua Landcare Research, 2021), and an inset locator map within Aotearoa New Zealand (National Topographic Office, 2012).

recorded over 2011–2019 (Orchard et al., 2020), which can create similar impacts to SLR including increased saltwater encroachment within the estuarine rivers.

The study area for this paper spans from the coastline to approximately 9.3 km inland based on the five–metre thickness contour line of the Christchurch Formation from Begg et al. (2015) implied by the study area boundary (Fig. 1). Within the 81.8 km^2 study area, the average ground elevation was 4.6 m above mean sea level (Land Information New Zealand, 2021) and the average of median groundwater level from 2016 to 2020 was 0.84 m below ground level (Bosserelle et al., 2023).

2.2. SI vulnerability mapping methods

SI vulnerability was assessed and mapped using two methods: (i) SI vulnerability tiers, within which the analytic solutions are applied, and (ii) GALDIT–SUSI. Both methods were applied in ArcGIS Pro (ESRI, 2022). The relative SLR scenarios considered were 0.5 m and 1.0 m, which were predicted to respectively occur in 2080 and 2120 with medium confidence at approximately the centre of the coastline within the study area (NZ SeaRise, 2022). These projections incorporate vertical land movements and are based on the Shared Socioeconomic Pathway 2–4.5 (i.e., the projected path under current policy settings) (Riahi et al., 2017).

2.2.1. SI vulnerability tiers and the analytic solutions

The SI vulnerability tiers developed in this study are based on the analytic solutions of Strack (1976), surface water salinity, and the freshwater head gradients between surface water and groundwater. The analytic solutions of Strack (1976), which resolved the position of the steady–state freshwater–saltwater interface in coastal aquifers, were developed further by Werner et al. (2012) to create SI vulnerability indicators under current conditions and future hydrological stresses including SLR. The modified versions of these equations to account for dispersion (Pool & Carrera, 2011) and sloping unconfined aquifers (Koussis et al., 2012) were not used as they were deemed unnecessary for a first-pass vulnerability analysis. Thus far, the analytic solutions have only been applied along the coast (i.e., not along riparian or estuary margins) and the results have not been spatially mapped using GIS (Mantoglou, 2003; Morgan & Werner, 2015; Morgan et al., 2013; Werner et al., 2012). An exception is Wriedt and Bouraoui (2009) that spatially plotted saltwater toe movement from an unstressed to a stressed state along the Spanish Mediterranean coast. The novelty of this study involves the application of the analytic solutions along the coast, estuary, and estuarine rivers in GIS to evaluate SI vulnerability in an unconfined aquifer and the development of SI vulnerability tiers. For this paper, the ocean, estuaries, and estuarine rivers are all considered surface water bodies and referred to as such hereafter. The analytic solutions assume a steady–state flow in a homogeneous and isotropic aquifer, a sharp freshwater–saltwater interface, negligible vertical flows compared to horizontal flows, negligible flow rates in the saltwater zone compared to those in the freshwater zone, and that the aquifer does not extend offshore and is bounded by an impervious base at the bottom (Strack, 1976). The methods below focus on the application of the analytic solutions along estuarine riverbanks (i.e., in a riparian setting).

There are several key differences between SI from the coast and riparian SI. These include full versus partial penetration of the surface water body into the aquifer, different surface water volumes at the river versus coastal boundaries, and temporal variation of surface water salinity (Setiawan et al., 2023). To the authors' knowledge, there are no specific analytic solutions for riparian SI. Here we propose the use of SI vulnerability tiers developed using the analytic solutions in riparian settings as a useful first–pass approximation of riparian SI vulnerability. This application requires additional simplifications such as ignoring the shallower penetration of estuarine rivers into the aquifer compared to the ocean. The application of analytic solutions along rivers essentially involved the substitution of sea parameters for river parameters.

The water budget for the problem domain adapted in an estuarine river setting (Fig. 2) includes distributed net recharge (accounting for infiltration, evapotranspiration, and distributed pumping), W_{net} [LT^{-1}], freshwater flow from aquifers inland of the landward boundary, q_b [L^{2}T^{-1}], and freshwater discharge at the surface water boundary, q_0 [L^{2}T^{-1}]. Other hydrogeological variables include freshwater head relative to mean surface water level, h_b [L], depth to aquifer base from mean surface water level, z_0 [L], distance from the surface water boundary to where fresh groundwater head is measured, x_b [L], saltwater wedge toe distance from the surface water boundary, x_T [L], and aquifer hydraulic conductivity, K [LT^{-1}]. The problem domain is divided into two zones: Zone 1 located inland of the toe (i.e., $x_b \geq x_T$) where the aquifer consists of freshwater only, and Zone 2 located from the toe towards the surface water body (i.e., $0 \leq x_b < x_T$) where the aquifer consists of saline or brackish water overlain by freshwater.

The Ghyben–Herzberg relation $z = h/\delta$, was used to determine whether groundwater level is measured in Zone 1 or 2, where z [L] is the depth to the interface from mean sea level (MSL) and h [L] is the freshwater head above MSL. In this application, the MSL was substituted with the mean surface water level. The dimensionless density ratio δ [–], is $\delta = (\rho_{sw} - \rho_f)/\rho_f$, where ρ_{sw} and ρ_f are surface water and freshwater densities [ML^{-3}], respectively. At the toe, it was considered that $h_b = z_0\,\delta$ (Morgan et al., 2013; Werner et al., 2012). Therefore, the freshwater head is measured in Zone 1 if $h_b > z_0\,\delta$ and Zone 2 if $h_b < z_0\,\delta$.

The W_{net} parameter was assumed to be zero as it was unknown for the study area. Ōtautahi Christchurch is a low rainfall area and most aquifer recharge originates from lateral inflows from an alpine-fed braided river north of the city (Stewart, 2012). Additionally, the study area is a city with extensive impermeable surfaces and substantial urban runoff; therefore, recharge from rainfall was assumed to be negligible. Urban pathways of groundwater recharge such as engineered stormwater basins and leakage from pipe networks (Lerner, 1990) were not considered.

In Zone 1, q_0 is given by (Morgan et al., 2013):

$$q_0 = \frac{K\left((h_b + z_0)^2 - (1+\delta)z_0{}^2\right) + W_{net}x_b{}^2}{2x_b} \tag{1}$$

In Zone 2, q_0 is given by (Morgan et al., 2013):

$$q_0 = \left(\frac{1+\delta}{\delta}\right)\frac{K}{2x_b}h_b{}^2 + \frac{W_{net}x_b{}^2}{2} \tag{2}$$

Where $W_{net} = 0$, x_T is given by (Morgan & Werner, 2015):

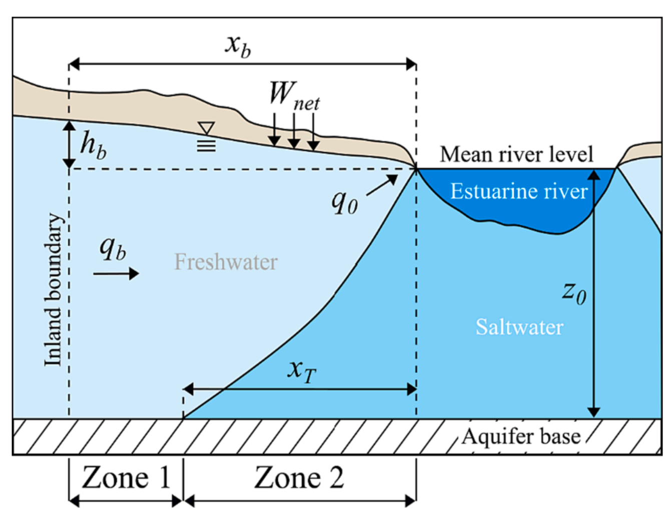

Fig. 2. onceptual diagram of a steady-state sharp interface in an unconfined aquifer with hydrogeological variables adapted in an estuarine river or riparian setting (adapted from Morgan et al., 2012; Werner et al., 2012).

$$x_T = \frac{K\delta(1+\delta)z_0^2}{2q_0} \tag{3}$$

SI along the coast has been classified as passive, passive–active, and active SI depending on the direction of groundwater flow in coastal settings (Werner, 2016). The conditions that trigger the onset of these different forms of SI were developed using the analytic solutions described above. The SI vulnerability assessment method developed in this study is related to the SI classifications of Werner (2016). These SI classifications of passive and active in an unconfined aquifer without recharge were extended to riparian settings by considering the freshwater head gradients between groundwater and the estuarine river (e.g., Setiawan et al., 2023). Adapted in a riparian setting, passive SI occurs when the aquifer freshwater head is greater than that in the river, groundwater flows against the direction of saltwater flow, and fresh groundwater discharge persists. On the other hand, active SI occurs when the river freshwater head is greater than that in the aquifer, groundwater flows inland with the direction of saltwater flow, and fresh groundwater discharge ceases. The onset of active SI is characterized by the drop of the freshwater head in the aquifer relative to that in the river and the cessation of fresh groundwater discharge. Under active SI, x_T is unable to be calculated due to unstable interface conditions (Morgan & Werner, 2015; Morgan et al., 2013).

Freshwater head in the surface water body, h_{fs} [L], is given by (adapted from Post et al., 2018):

$$h_{fs} = \frac{\rho_{sw}h_{sw} - (\rho_{sw} - \rho_f)z_{sw}}{\rho_f} \tag{4}$$

Where h_{sw} [L] is the surface water level relative to the local vertical datum (LVD) and z_{sw} [L] is the surface water bed elevation relative to the LVD.

Freshwater head in the aquifer, h_{fa} [L], is given by (Post et al., 2018):

$$h_{fa} = \frac{\rho_a h_a - (\rho_a - \rho_f)z}{\rho_f} \tag{5}$$

Where ρ_a [ML^{-3}] is the average groundwater density over the water column, h_a [L] is the groundwater level relative to the LVD, and z [L] is the well bottom elevation relative to the LVD.

The freshwater head in the aquifer relative to that in the surface water body, or p [L], was a criterion used in the SI vulnerability assessment and given by:

$$p = h_{fa} - h_{fs} \tag{6}$$

The determination of p before applying the analytic solutions is important to avoid a false positive q_0 in Equations (1) and (2) under conditions of active SI, whereby $h_{fa} \leq h_{fs}$.

This study extends Werner et al. (2012) by developing a tiered system that categorizes SI vulnerability. Tier 1 describes maximum SI vulnerability, where the surface water body adjacent to the aquifer is brackish or saline (>1000 kg m^{-3}) and active SI occurs based on the conditions outlined above and in Table 1. Tier 2 describes moderate SI vulnerability, where the surface water body adjacent to the aquifer is brackish or saline and passive SI occurs. In this tier, x_T values could be calculated. The further inland the wedge toe is located, the higher the vulnerability. Finally, Tier 3 describes the least vulnerable category, where the adjacent surface water body is fresh (≤1000 kg m^{-3}) and no SI occurs. The workflow is provided in Fig. S2 within the Supplementary Materials. The SI vulnerability assessment was re–run for each sea level scenario (i.e., current sea level, 0.5 m and 1.0 m SLR). The fixed head boundary condition was adopted in this study under SLR. Only the average or median of surface water and groundwater levels were applied in the analysis and tidal amplitudes were not considered.

In brackish or saline river reaches where the fluid density was greater than 1000 kg m^{-3} (or salinity > 1 ppt), a static ρ_{sw} was applied to calculate h_{fs}, q_0, and x_T. In the current application, a static ρ_{sw} value of 1009 kg m^{-3} was used, derived from the average ρ_{sw} along the brackish river reaches (i.e., > 1000 kg m^{-3}) in the Ōtākaro and Ōpāwaho Rivers across all sea level scenarios. For applications along the Ihutai Estuary and the coast, a static seawater density of 1025 kg m^{-3} was used as the ρ_{sw} value. The analytic solutions of Strack (1976) assume a sharp freshwater–saltwater interface with no mixing zone and therefore the calculated x_T represents a saltwater toe with the same fluid density as the surface water body. For example, if a ρ_{sw} value of 1009 kg m^{-3} was used, the calculated x_T would also represent a saltwater toe with a density of 1009 kg m^{-3}. Therefore, if spatially variable river densities were considered in the x_T calculation, the resulting x_T values would also represent saltwater toes of variable densities along the river. A static ρ_{sw} value was hence chosen to be able to compare the vulnerability of sites along the river. Additionally, this allows for data parsimony as fluid density across the river length is often unknown. However, the upstream reach of saltwater during high tide is easier information to obtain, and a static ρ_{sw} value can be applied downstream of a location (i.e., where the river is brackish to saline).

The sources of data for individual equation terms are detailed in Text S1, and the GIS flowchart to apply the analytic solutions is shown in Fig. S3, both within the Supplementary Materials. Aquifer property values as well as outputs from the hydrodynamic model of Orchard and Measures (2016), which modelled surface water behaviour under current sea level and SLR (described in Text S4 within the Supplementary Materials), were used in the SI vulnerability assessment to categorize areas along surface water banks into vulnerability tiers (Table 1). If hydrodynamic model results are unavailable in other studies, results derived from surface water analytical solutions can be used to estimate saltwater encroachment conditions, which can feed into the SI vulnerability mapping approach proposed here. In Tier 2 areas where passive SI occurred, x_T was calculated based on Equation (3) using a Python script. Open–source Python libraries including Pandas (McKinney, 2010) and Matplotlib (Hunter, 2007) were used. The projection of x_T was limited to 250 m perpendicular to the surface water boundaries to reduce the complexity of the output maps.

Table 1
SI vulnerability tiers, classifications, and conditions where $W_{net} = 0$.

SI vulnerability tier	Surface water density, ρ_{sw} (kg m^{-3})	Conditions	SI classification
Tier 1 (maximum vulnerability)	> 1000	$p \leq 0$	Active
Tier 2 (moderate vulnerability)	> 1000	$p > 0$, $q_0 > 0$	Passive
Tier 3 (least vulnerable)	≤ 1000	N/A	No SI

2.2.2. GALDIT–SUSI

GALDIT–SUSI (Kazakis et al., 2019) is an extension of an earlier seawater intrusion vulnerability indexing approach called GALDIT (Lobo-Ferreira et al., 2007). GALDIT assesses SI vulnerability based on a weighted sum of six hydrogeological factors perceived to influence SI vulnerability and its name is an acronym based on these hydrogeological factors: *G*roundwater occurrence (aquifer type), *A*quifer hydraulic conductivity, *L*evel of groundwater relative to MSL, *D*istance from the coast, *I*mpact of existing seawater intrusion, and *T*hickness of aquifer.

GALDIT–SUSI extends GALDIT by adding Superficial Saltwater Intrusion (SUSI) factors to consider surface water bodies as sources for groundwater salinization, namely vadose zone hydraulic conductivity, elevation or bathymetry, and distance from torrents, rivers, wetlands, and lagoons (Kazakis et al., 2019). The values for each factor are categorized into vulnerability groups of low to high associated with risk ratings. Each hydrogeological factor was initially assigned an importance weight (Table S1 in the Supplementary Materials) determined using the Analytic Hierarchy Process or AHP (Saaty, 1990), following the methodology of Kazakis et al. (2019). Within the AHP, a pairwise comparison matrix (Table S2 in the Supplementary Materials) was used to compare the perceived significance of one factor against the other in causing SI. The distance from torrents factor was removed in this analysis as there were no torrents in the study area and the importance weights were recalculated in the pairwise comparison matrix. The data sources for each hydrogeological factor and GALDIT-SUSI steps in GIS are elaborated in Text S2 and Text S3, respectively, within the Supplementary Materials.

To implement GALDIT–SUSI, each factor layer was reclassified into its risk rating based on the values in Table S1. Then, the initial GALDIT–SUSI index, I, was calculated using Equation (7):

$$I = \frac{\sum_{i=1}^{12} W_i \bullet R_i}{\sum_{i=1}^{12} W_i} \quad (7)$$

Where W_i is the initial weight of individual factors derived from AHP and R_i is the risk rating assigned to each class shown in Table S1.

Then, a sensitivity analysis (Napolitano & Fabbri, 1996) was carried out to determine the contribution of each factor to the final vulnerability map by computing its effective weight, E_i, using Equation (8) (Kazakis et al., 2019):

$$E_i = \left(\frac{W_i \bullet R_i}{I}\right) \times 100 \quad (8)$$

An effective weight for each factor was then generated for each sea level scenario. The final weights derived from the average of mean effective weights for each factor across all sea level scenarios, $\overline{E}_i$, were used to calculate the final GALDIT–SUSI index using Equation (9) (Kazakis et al., 2019):

$$GALDITSUSI = \frac{\sum_{i=1}^{12} \overline{E}_i \bullet R_i}{\sum_{i=1}^{12} \overline{E}_i} \quad (9)$$

3. Results

3.1. SI vulnerability tiers and the analytic solutions

The SI vulnerability tiers based on surface water salinity, surface water-groundwater freshwater head gradients, and the analytic solutions for the steady–state freshwater–saltwater interface in an unconfined aquifer (Strack, 1976; Werner et al., 2012) were applied in a GIS environment along surface water bodies (i.e., ocean, estuary, and river margins) under current sea level, 0.5 m and 1.0 m SLR to assess SI vulnerability.

Under the current sea level, the proportion of areas categorized as Tier 1 (i.e., maximum vulnerability) was 31 % along the Ōtākaro River and 38 % along the Ōpāwaho River (Fig. 3). Less than 10 % of the areas along both rivers were categorized as Tier 2 (i.e., moderate vulnerability). Further, more than half of the areas along both rivers were categorized as Tier 3 (i.e., least vulnerable to SI). Meanwhile, areas around the Ihutai Estuary experienced the greatest proportion of Tier 1 vulnerability (i.e., 98 %) compared to other surface water bodies. Most areas along the coastline (i.e., 76 %) experienced Tier 1 vulnerability in the current sea level scenario.

The proportion of areas experiencing Tier 1 vulnerability along all surface water bodies increased with rising sea levels. A 22 % increase in Tier 1 areas was observed along the Ōtākaro River under 0.5 m SLR, and a further 22 % increase was observed under 1.0 m SLR. The expansion of Tier 1 areas along the Ōpāwaho River was less than the Ōtākaro River at 7 % under 0.5 m SLR, and a further 15 % increase under 1.0 m SLR. All areas along the Ihutai Estuary experienced Tier 1 vulnerability under both SLR scenarios. Nearly all areas along the coast experienced Tier 1 vulnerability under 0.5 m SLR, which expanded to 100 % under 1.0 m SLR.

In areas experiencing Tier 2 vulnerability, x_T values were calculated. Along the Ōtākaro, x_T ranged from 90 to 5140 m across all sea levels (Table 2). Meanwhile, the x_T along the Ōpāwaho ranged from 7 to 6050 m across all sea levels. The x_T values along the Ihutai ranged from 330 to 2873 m under the current sea level and there were no Tier 2 areas in both SLR scenarios. The greatest range of x_T was found along the coast

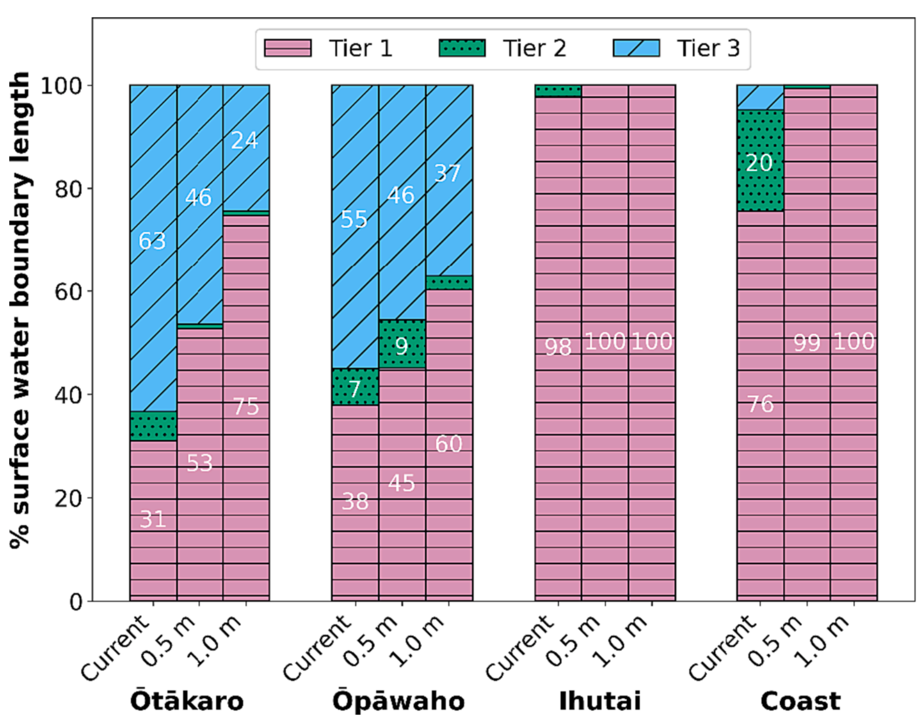

Fig. 3. SI vulnerability tiers as a percentage of surface water boundary length under current sea level, 0.5 m SLR, and 1.0 m SLR scenarios.

Table 2
Minimum and maximum x_T along surface water bodies under various sea level scenarios. None values are due to the inability to calculate x_T in Tier 1 and the lack of Tier 2 areas.

Surface water body	x_T (m)					
	Current sea level		0.5 m SLR		1.0 m SLR	
	Min	Max	Min	Max	Min	Max
Ōtākaro	275	1007	90	641	4372	5140
Ōpāwaho	7	207	12	6050	86	1353
Ihutai	330	2873	None	None	None	None
Coast	60	6580	1424	1424	None	None

(60 to 6580 m) across the sea level scenarios compared to other surface water bodies.

As saltwater encroached further up the estuarine rivers and the hydraulic head at the river boundary increased with rising sea levels, areas experiencing Tier 1 also grew upstream (Fig. 4 and Fig. 5). True left refers to the left-hand side of the river when facing downstream and true right is vice versa (Fig. 5). Most Tier 2 areas were observed to occur in between Tier 1 areas. Within Tier 2 sites, x_T greater than 250 m were not projected inland from the surface water boundary to reduce the complexity of the maps in Fig. 4. The areas not defined as Tier 1 or Tier 2 within Fig. 4 and Fig. 5 were categorised as Tier 3 (least vulnerable). The areas with the least SI vulnerability were adjacent to the most upstream reaches of both rivers, where the rivers were fresh.

Under SLR, the fresh groundwater head inland remained the same despite rising surface water levels due to the fixed head inland boundary condition, while saltwater encroachment also increased further up estuarine rivers. As a result, the freshwater head in the aquifer relative to that at the surface water, or p, decreased with SLR (Fig. 6), causing more areas of the aquifer to have freshwater head below that at the river (i.e., $p < 0$) and active SI conditions (Tier 1 or maximum SI vulnerability). Where the surface water adjacent to the aquifer is above 1000 kg m^{-3} and $p > 0$, passive SI occurred (Tier 2 or moderate vulnerability) and x_T was displayed. The closer to zero the p, the larger the x_T (i.e., the further inland the saltwater wedge toe) (Fig. 6). Upstream of the Tier 1 and 2 areas, there were areas where $p < 0$ in all sea level scenarios. However, the river water adjacent to these areas was fresh (Fig. 5) and therefore not considered vulnerable to SI (Tier 3).

3.2. GALDIT–SUSI

GALDIT–SUSI, a weighted indexing method aiming to assess SI vulnerability that accounts for surface water bodies as salinity sources, was applied in a GIS environment. Fig. S4 shows the reclassified GALDIT–SUSI factors (based on their risk ratings in Table S1) that changed with SLR, while Fig. S5 shows those that were static despite SLR (both figures are in the Supplementary Materials). As expected, the overall GALDIT–SUSI risk rating of factors that changed with SLR increased with rising sea levels (Fig. S4).

According to the present application of the GALDIT–SUSI method, the three most important factors in determining SI were groundwater occurrence (aquifer type), elevation, and groundwater level. The importance of factors can change in different study areas depending on site–specific conditions. The original factor weights derived from the AHP in Table S2 changed following the sensitivity analysis (Equation (9) where the effective weights were derived (Table S3). The larger the risk rating multiplied by the weight, the larger the increase in effective weight. Compared to the original factor weights (Table S2), the final weights of groundwater occurrence (aquifer type), elevation, thickness of aquifer, and distance from lagoons and rivers increased (ordered from the largest to the smallest increase) (Table S3). Meanwhile, the final weights of the other factors decreased to compensate for these increases. The final weight of groundwater occurrence (aquifer type) had the largest increase as the unconfined aquifer was assigned a high risk rating

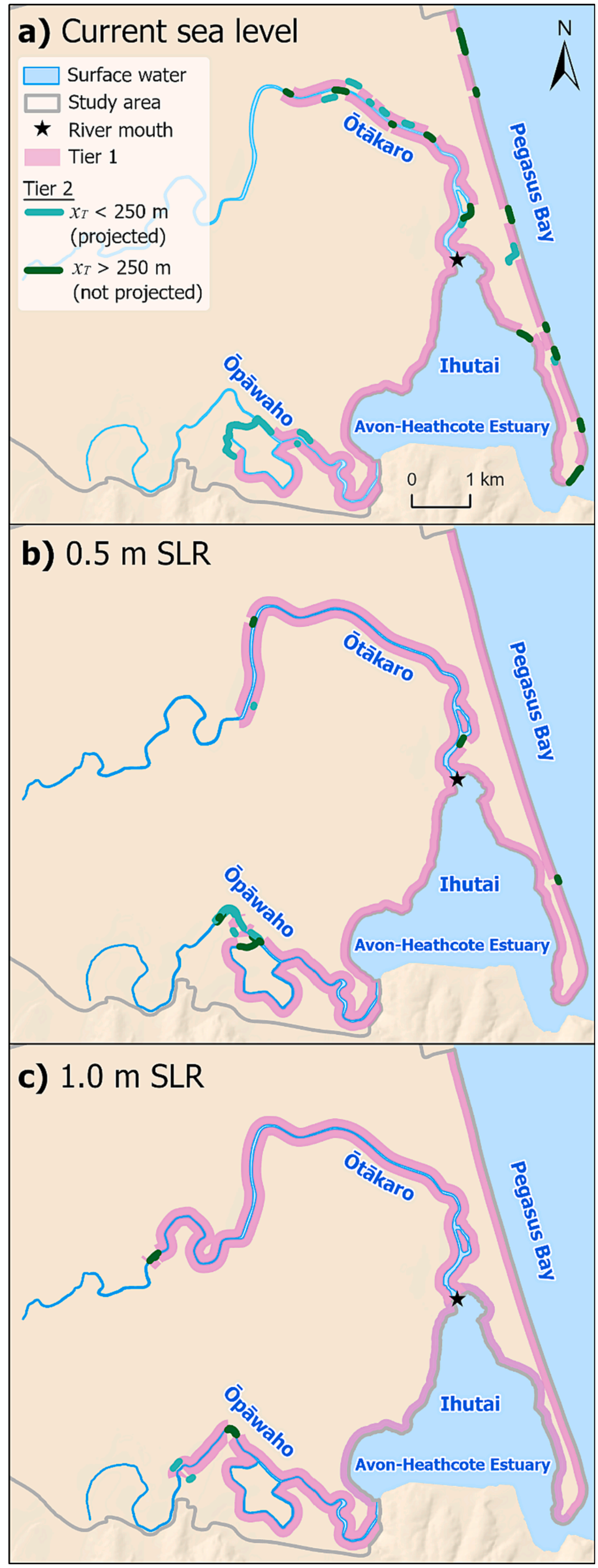

Fig. 4. SI vulnerability assessment using analytic solutions under a) current sea level, b) 0.5 m SLR, and c) 1.0 m SLR. The x_T along rivers relates to a fluid density of 1009 kg m^{-3} and the x_T along the estuary and ocean relates to a fluid density of 1025 kg m^{-3}. The maximum x_T displayed is 250 m from the surface water boundary.

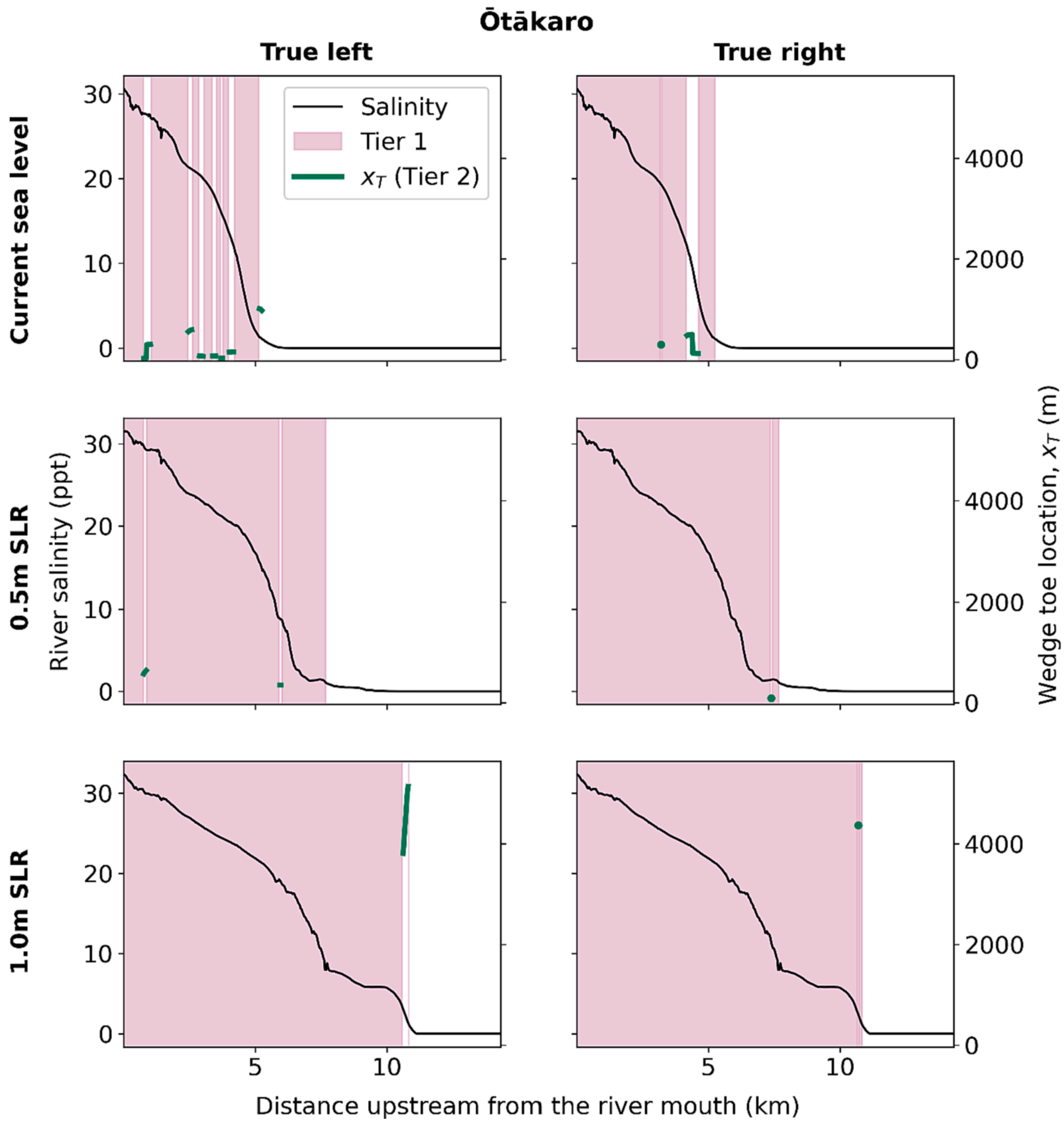

Fig. 5. Ōtākaro River salinity, Tier 1 areas, and calculated x_T (of 1009 kg m^{-3}) in Tier 2 areas on the true left and true right under current sea level, 0.5 m, and 1.0 m SLR scenarios.

of 7.5; this factor already had one of the highest weights (Table S2). Therefore, its risk rating (13.9 %) multiplied by its weight (uniform value of 7.5 throughout the study area) resulted in the highest effective weight.

The GALDIT–SUSI vulnerability index derived from Equation (9) ranged from 3.6 to 8.6 across all sea level scenarios. The index was equally split into five tiers of very low (3.6 to 4.6), low (4.6 to 5.6), medium (5.6 to 6.6), high (6.6 to 7.6), and very high (7.6 to 8.6) vulnerability aligned with Kazakis et al. (2019) (Fig. 7).

Under the current sea level, areas with very high vulnerability were observed around the Ihutai estuary and the Ōtākaro and Ōpāwaho river mouths (Fig. 7a). Areas with high vulnerability were observed along the coast, around the estuary, up the Ōtākaro river, and the lower reach of the Ōpāwaho river. Medium vulnerability was observed further inland from the Ōtākaro river and the estuary, at Travis Wetland (the last large freshwater wetland in Ōtautahi), Horseshoe Lake (see Fig. 1 for place names), and around the lower reach of the Ōpāwaho. Areas between the Ōtākaro and Ōpāwaho rivers had low vulnerability. Meanwhile, areas near the inland study area boundary had the lowest vulnerability.

In the SLR scenarios, areas with very high vulnerability increased around the estuary, further up the Ōtākaro and Ōpāwaho river mouths toward low-lying land (Fig. 8b and c). Under SLR, GALDIT-SUSI vulnerability increased along the coast, at Travis Wetland, Horseshoe Lake, and further inland of the estuary and rivers toward low-lying topography. Low vulnerability areas between the two rivers were further reduced in size with rising sea levels.

Areas with high risk ratings often overlapped for different factors (Fig. S4). Some examples include: (i) Travis Wetland (location outlined in Fig. 1) rated as high risk due to low groundwater level, low elevation, and is a wetland, which is seen as a risk in itself, and (ii) the Ōtākaro river mouth area rated as high risk due to low groundwater level, low elevation, existing SI, and located near lagoons, wetlands, and rivers. The GALDIT-SUSI vulnerability of these areas increased with rising sea levels.

SLR increased the mean and the median of GALDIT–SUSI vulnerability ratings and shifted the data distribution toward higher vulnerability values (Fig. 8). Under the current sea level, the GALDIT–SUSI vulnerability index histogram has a right–skewed distribution with most cells categorised as low vulnerability. Under 0.5 m SLR, most cells were still in the low vulnerability category, however, the distribution shifted toward the centre and was less skewed. Meanwhile, in the 1.0 m SLR scenario, most cells were in the medium vulnerability category and the

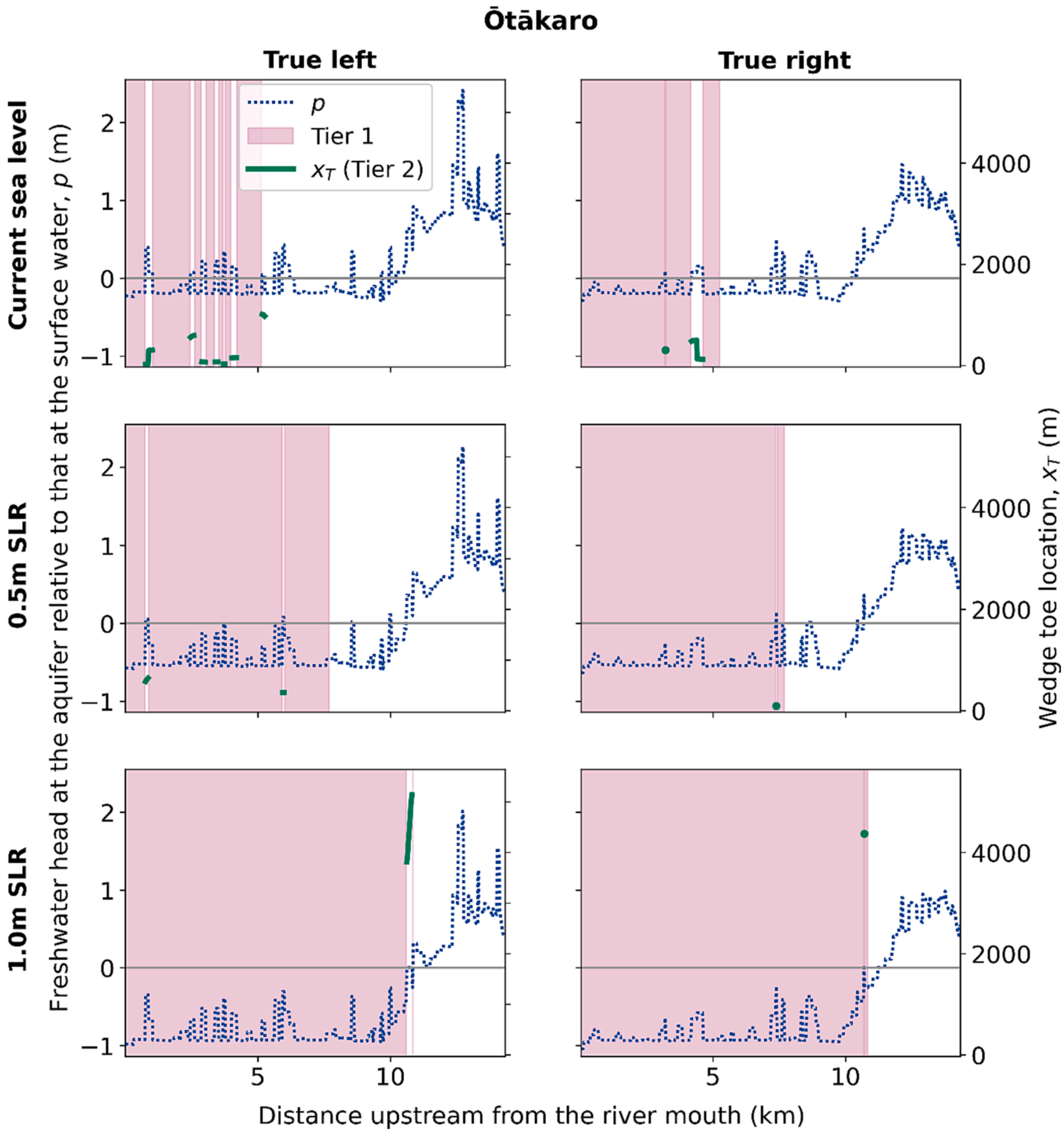

Fig. 6. Calculated p (at $x_b = 50$ m), Tier 1 areas, and x_T in Tier 2 areas along the true left and true right of the Ōtākaro River under current sea level, 0.5 m, and 1.0 m SLR scenarios.

distribution can be described as bimodal.

3.3. Comparison of SI vulnerability tiers and GALDIT-SUSI

The comparison of SI vulnerability along the Ōtākaro based on the SI vulnerability tiers and GALDIT-SUSI is shown in Fig. 9. Both methods showed that SI vulnerability increased with SLR and decreased upstream of the river mouth. There was no apparent correlation between the SI vulnerability tiers and the GALDIT–SUSI index.

4. Discussion

4.1. SI vulnerability tiers and the analytic solutions

This study showed that SI vulnerability assessments based on the analytic solutions can be applied at a large scale in a GIS framework and not limited to one representative cross–section per aquifer like previous applications (e.g., Beebe et al., 2016; Morgan & Werner, 2015; Morgan et al., 2013; Werner et al., 2012). The mapping of SI vulnerability tiers provides a spatial nuance of vulnerability, allowing high–risk areas to be narrowed down, which may be easier to achieve compared to investigating different parameter ranges for an aquifer (e.g., Werner & Simmons, 2009; Werner et al., 2012). Additionally, SI vulnerability tier mapping allows for site–specific parameter combinations (e.g., groundwater level, river salinity and level, hydraulic conductivity) to estimate vulnerability along kilometres of surface water boundaries, which may be difficult without mapping approaches. For example, this study assessed SI vulnerability along 70 km of surface water boundary across three sea level scenarios.

The increase in river head and salinity under SLR drove the increase in aquifer areas experiencing active SI (i.e., Tier 1 or maximum vulnerability) upstream of estuarine rivers, which was expected based on previous studies (e.g., Bhuiyan & Dutta, 2012; Tully et al., 2019). In addition, the increase in the estuary and ocean heads with rising sea levels also increased SI vulnerability along the estuary and the coast, following earlier research (e.g., Passeri et al., 2015; Werner & Simmons, 2009). The extent of active SI sites was exacerbated by the fixed head inland boundary condition under SLR, which is likely to occur in

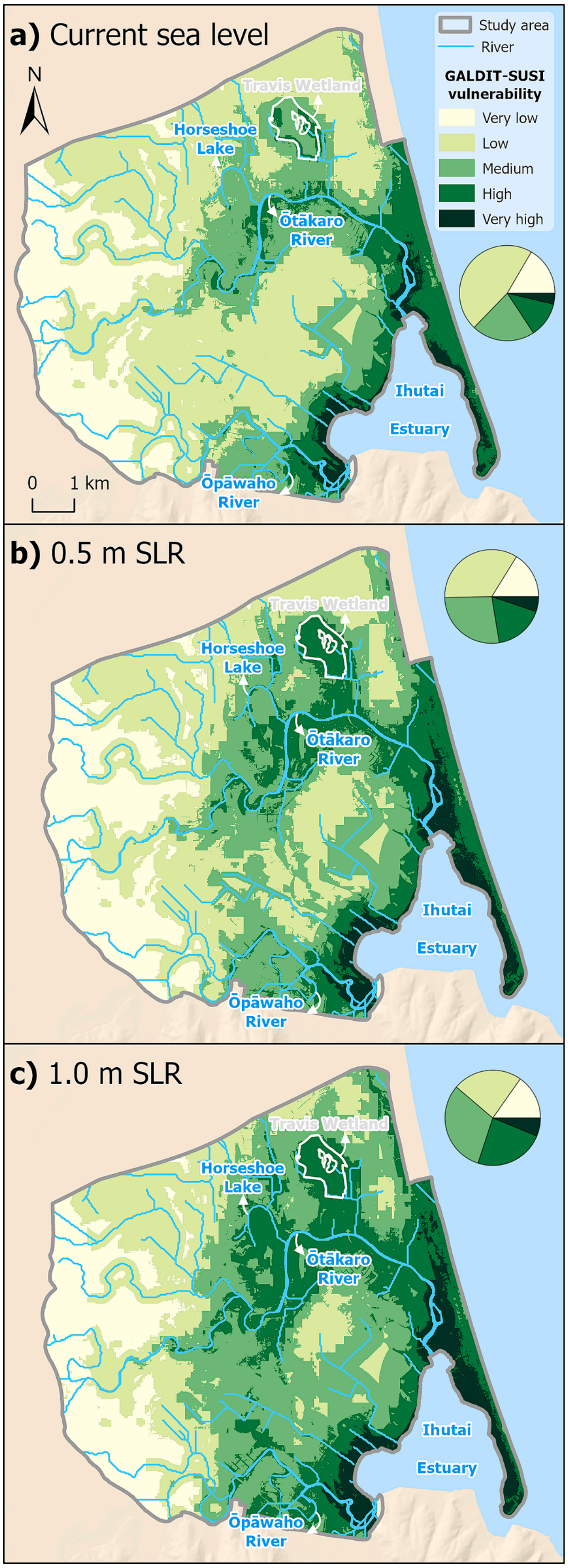

Fig. 7. GALDIT–SUSI vulnerability maps and pie charts of vulnerability groups under a) current sea level, b) 0.5 m SLR, and c) 1.0 m SLR scenarios.

extensively drained and low–lying topography–limited systems (i.e., the ability for the water table to rise with SLR is limited by its proximity to the ground surface) such as the study area (Michael et al., 2013). This boundary condition resulted in decreased p (i.e., groundwater–surface water freshwater head gradients) and groundwater flux to the river with rising sea levels, and the most severe SI scenario (Werner & Simmons, 2009).

Where passive SI occurred (i.e., moderate or Tier 2 vulnerability), some of the calculated x_T reached kilometres inland from the riverbank, although $x_T > 250$ m was not displayed in the maps (Fig. 4). For example, the maximum x_T calculated along the Ōtākaro was 5140 m from the river boundary occurring under 1 m SLR (Table 2 and Fig. 5). These x_T calculations can be useful to determine relative SI vulnerability along surface water boundaries as a first–pass assessment. However, the assumptions within the analytic solutions (noted in Section 2.2.1) resulted in toe calculations that are not generally comparable to field conditions (Werner et al., 2013), particularly in riparian settings. Areas of active and passive SI may be more likely to represent average field conditions, although further investigation is required for verification. In coastal settings, Beebe et al. (2016) found that the analytic solutions correctly predicted SI in 60 % of wells across nine aquifers owing to their simplifying assumptions that were mismatched with more complex field conditions. To apply the analytic solutions in riparian settings, there were further simplifications. For example, the river was assumed to be fully penetrating the aquifer (i.e., the riverbed was assumed as equal to the aquifer base), and the river salinity was assumed uniform downstream of the upper saltwater encroachment extent, even in reaches closely approaching fresh conditions (e.g., ρ_{sw} of 1001 kg m^{-3}) for comparability purposes.

It is important to note that the riverbed was not assumed equal to the aquifer base in the calculation of p. Instead, the average surface water bathymetry was used to calculate freshwater heads. If all surface water bodies were assumed to fully penetrate the aquifer, active SI (i.e., $p < 0$) would occur along all brackish or saline surface water bodies across all sea level scenarios, except for the Ōtākaro at current sea level and the Ōpāwaho at current sea level and 0.5 m SLR.

4.1.1. Alternative methodologies

This subsection discusses approaches to applying the SI vulnerability tiers in a GIS environment that are alternative to the method proposed and used in this paper, including a simplified version and using analytic solutions that consider a positive net recharge. The visualization of the saltwater toe is also discussed.

For a simpler and more rapid application of the SI vulnerability tiers, the x_T calculations can be omitted. The results of this simplified method would therefore show locations of active and passive SI without the x_T calculations, as well as no SI (Tier 1, 2, and 3, respectively). The data for the x_T calculations such as K, z_0, and W_{net}, would therefore not be required in the simplified method. Instead, p can be used to determine relative vulnerability within Tier 2 areas. As p decreases, SI vulnerability increases (as shown by the x_T response in Fig. 6). In cases where the river levels are only known at two locations, the river levels between them may be interpolated. If the change in surface water parameters under SLR is known, the simplified method can also be applied to assess SI vulnerability under SLR.

In this study, it was assumed that W_{net} equalled zero. However, in other areas where W_{net} cannot be assumed as zero, the SI vulnerability tiers can be modified to consider $W_{net} > 0$ in unconfined aquifers. Positive net recharge allows the formation of a groundwater mound, and the distance from the surface water boundary to its peak is x_n [L], which is equal to q_0/W_{net}. Passive–active SI occurs when the saltwater toe reaches the groundwater mound (Werner, 2016). In this case, fresh groundwater discharge toward the river persists but there is active SI on the landward side of the mound. A threshold condition for the transition from passive SI to passive–active SI is when $q_0 = \sqrt{W_{net}K\delta(1+\delta)}z_0$, which results in

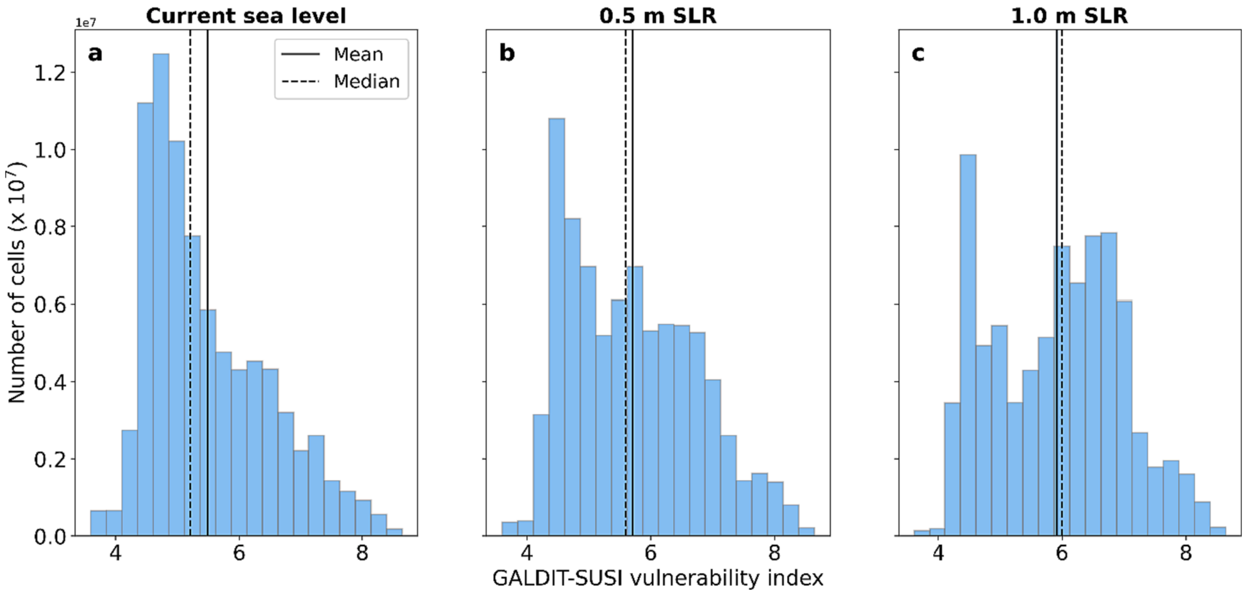

Fig. 8. GALDIT–SUSI vulnerability index histograms under a) current sea level, b) 0.5 m SLR, and c) 1.0 m SLR.

an incalculable x_T. It is important to note that the x_T equation used will be different from Equation (3), considering $W_{net} > 0$ (see Werner et al., 2012). Where $W_{net} > 0$ and $x_b < x_n$, the SI vulnerability tiers in Table 3 can be considered.

As mentioned, x_T greater than 250 m was not projected from the surface water boundary to reduce the complexity of the output maps. The larger the maximum x_T displayed, the further inland the x_T is projected and the longer the x_T line becomes. Additionally, the display of x_T was also complicated by meandering river channels as the x_T points were projected perpendicular from the river boundary to the true left or true right side of the river. An example is shown in Fig. 10 a and b, where the x_T is projected on the true right side of the Ōpāwaho up to 500 m and 1000 m, respectively. It would be difficult to ascertain which river reach the x_T is projected from without the arrow annotations. To avoid this complexity, the maximum x_T display was chosen as 250 m in the current study, however, users can apply other distances as they see fit.

4.2. GALDIT–SUSI

The weight of each GALDIT–SUSI factor contributing to the final vulnerability index was arguably subjective and arbitrary. Kazakis et al. (2019) postulated that the AHP and sensitivity analysis used to assign GALDIT–SUSI factor weights were robust and representative of a modified GALDIT approach that accounts for surface water bodies as SI sources. However, AHP was created for decision–making based on personal judgements (Saaty, 1990) and therefore is inherently subjective. For example, in Table S2, the factor groundwater occurrence (aquifer type) was considered of moderate importance over aquifer hydraulic conductivity (therefore the intersection of row 1 and column 2 was assigned the value of 3), and extremely important over the impact of existing SI (therefore the intersection of row 1 and column 5 was assigned the value of 9). Arguably, there was no physical basis for the assignment of factor importance within the GALDIT–SUSI method. Additionally, Kazakis et al. (2019) contended that the sensitivity analysis validated the factor weights and overcame the subjectivity involved in the AHP. Since the basis of the AHP was subjective and arbitrary, we argue that the sensitivity analysis also did not overcome the subjectivity involved.

Despite the subjectivity of GALDIT–SUSI, it can be useful to compile the surface water and hydrogeological information needed for this method and that could affect SI vulnerability at specific sites (Cook et al., 2013; Jiao & Post, 2019). For example, the impact of existing SI (i.e., groundwater specific conductance) can provide valuable information on where existing conditions have already resulted in SI, which can be exacerbated under future SLR and decreased groundwater levels relative to surface water levels (Setiawan et al., 2023; Werner & Simmons, 2009). However, this factor was considered the least important in the present application of GALDIT–SUSI. The selection of some GALDIT–SUSI factors was based on established hydrogeological relationships such as groundwater level relative to MSL; the lower the groundwater level relative to MSL, the higher the risk for SI (Werner et al., 2012). Additionally, low–elevation areas are most likely to be artificially drained, which short–circuits hydrological flows and has been shown to compound SLR effects to increase SI vulnerability (Bhattachan et al., 2018). However, the methods to rank and amalgamate the factors into one overall vulnerability index are inherently subjective and lack a hydrogeological basis.

4.3. Comparison of SI vulnerability tiers and GALDIT–SUSI

To assess SI vulnerability, the tiered approach considered surface water conditions and therefore required current and future estimates of surface water parameters under SLR, such as the saltwater encroachment extent upstream of rivers. An exception was the ocean, as typical values were considered. Therefore, the application of the SI vulnerability tiers are limited to the surface water bodies with sufficient data (e.g., salinity and level). On the other hand, GALDIT–SUSI did not require these data as it does not account for surface water behaviour. GALDIT-SUSI considered all surface water bodies covered by the GIS data as potential salinity sources that increase vulnerability, including the tributaries far inland from the coast and those without salinity and level data. In this application, the tiered approach assessed SI vulnerability along the margins of surface water bodies covered within the hydrodynamic model outputs of Orchard and Measures (2016), while GALDIT–SUSI assessed SI vulnerability at a larger scale, i.e., across the study area by considering all surface water bodies as potential sources of vulnerability.

While the results of the SI vulnerability tiers and the analytic solutions can be conceptualized as physical phenomena (e.g., active and passive SI, saltwater toe position), the GALDIT–SUSI index cannot be conceptualized physically. The SI vulnerability tiers and the analytic solutions were based on physical relationships of hydrogeological parameters that impact SI, while the GALDIT–SUSI index was based on the perceived importance of selected parameters that may relate to SI. The

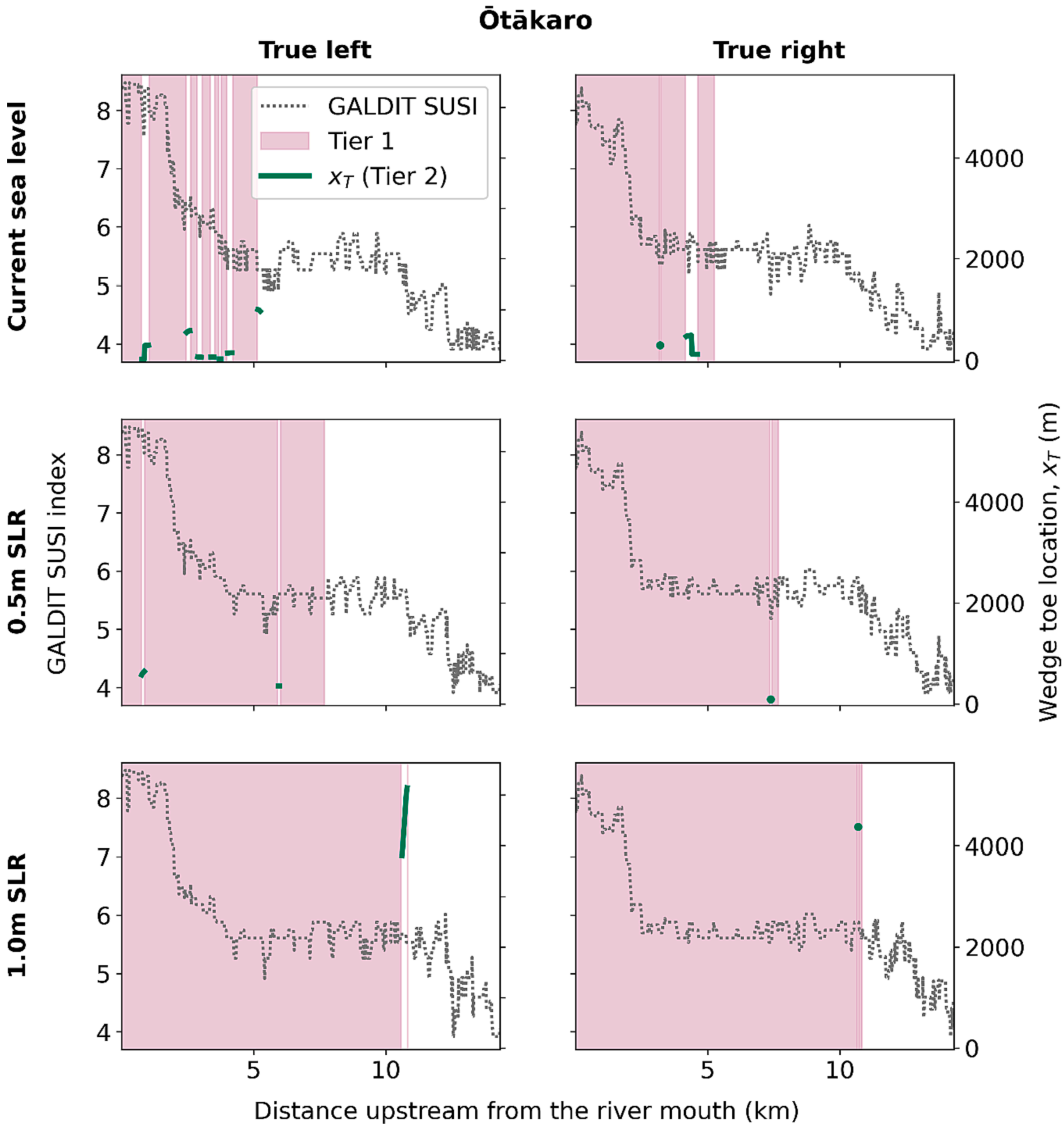

Fig. 9. GALDIT–SUSI and analytic solutions comparison on the true left and true right of the Ōtākaro (at $x_b = 50$ m) under current sea level, 0.5 m and 1.0 m SLR.

subjective processes involved in GALDIT–SUSI include the selection of factors, the grouping of factor values, the assignment of risk rating for each factor value group, and the pairwise comparison matrix in AHP (i.e., the assignment of factor weighting based on the perceived importance of one factor over the others).

The SI vulnerability maps from both methods may be easily understood, however, the reader needs to grasp basic SI concepts such as the saltwater toe location to interpret the vulnerability maps created using the analytic solutions. Additionally, both methods required GIS skills, however, the analytic solutions may also require Python scripting skills to apply the equations efficiently.

Many manual steps were involved in visualising the SI vulnerability tiers via the analytic solutions, and therefore there was more room for operator mistakes compared to GALDIT–SUSI. Additionally, the ease of analytic solutions application depended on the river geometry. The more complicated the shape (e.g., meandering channels), the more steps were required to visualise the vulnerability tiers. The application of GALDIT–SUSI required many steps; however, these would be easier to automate as there was no manual editing involved to visualise vulnerability.

Table 3
SI vulnerability tiers, classifications, and conditions where $W_{net} > 0$ and $x_b < x_n$.

SI vulnerability tier	Surface water density, ρ_{sw} (kg m^{-3})	SI classification	Conditions
Tier 1 (maximum vulnerability)	> 1000	Active Passive–active	$p \leq 0$, $q_0 \leq 0$ $p > 0$, $q_0 \leq \sqrt{W_{net}K\delta(1+\delta)}z_0$
Tier 2 (moderate vulnerability)	> 1000	Passive	$p > 0$, $q_0 > \sqrt{W_{net}K\delta(1+\delta)}z_0$
Tier 3 (least vulnerable)	≤ 1000	No SI	N/A

4.4. Implications

Ōtautahi Christchurch is comparable to many coastal cities worldwide built on drained swampland that face growing challenges in groundwater management under climate change (Barlow & Reichard, 2010; Mancini et al., 2020; Renken et al., 2005). Increased saltwater encroachment up rivers due to relative SLR exposed new areas of the aquifer to saltwater, which increased SI vulnerability upstream. Drainage infrastructure, installed to keep groundwater sufficiently deep below ground for city–building purposes, increase SI vulnerability as they keep groundwater at a constant level, reduces freshwater flows to counter SI, and inadvertently salinizes groundwater (Bhattachan et al., 2018; Werner & Simmons, 2009; Werner et al., 2012). Shallow groundwater salinization in an urban context has cascading impacts on subsurface infrastructure, municipal assets (e.g., wastewater treatment

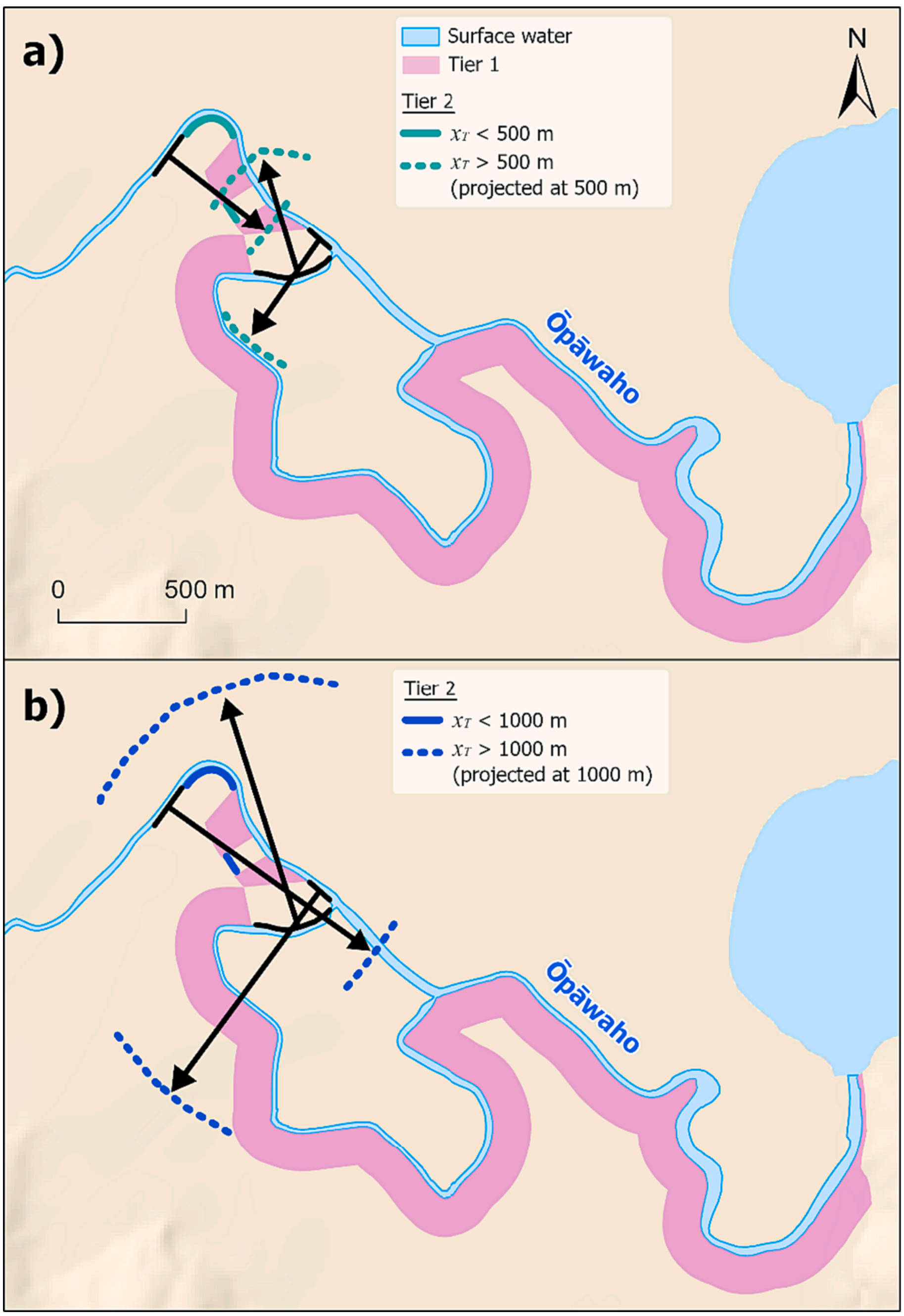

Fig. 10. SI vulnerability tiers along the true right of the Ōpāwaho under 0.5 m SLR with maximum projected x_T of a) 500 m and b) 1000 m.

plants), parks and reserves, and increases the risk of deep groundwater salinization under downward hydraulic gradients (Setiawan et al., 2022b). The feasibility and efficacy of freshwater management measures (e.g., surface water flow augmentation) and engineered surface water and groundwater structures to mitigate riparian SI in urban contexts, along with their ecological feedback, can be considered for individual sites (White & Kaplan, 2017).

4.5. Limitations and recommendations for future research

The proposed SI vulnerability tiers are limited in several ways. First, there is the lack of consideration of riverbed and aquifer hydraulic conductivity in determining active or passive SI. This may be resolved by considering the mixed convection ratio described in Werner et al. (2012), which considers aquifer hydraulic conductivity. Second, the steady-state sharp-interface equations of Strack (1976) assume an idealized aquifer and have inherent limitations, which are listed in Section 2.2.1. The application of these equations in riparian settings adds further assumptions. However, the purpose of this tiered approach is to approximate first-pass riparian SI vulnerability, which is a relative measure. Further, the proposed method applies a static surface water density in brackish or saline river reaches. The ease of analytic solutions application depended on river geometry; the more meandering the river channel, the more steps are required to visualise the vulnerability tiers. Finally, the developed approach does not consider saltwater intrusion due to paleoseawater, episodic coastal floods, or where surface water overtops riverbanks.

The suitability of SI vulnerability tiers and analytic solutions in assessing SI vulnerability from surface water bodies can be further investigated through numerical modelling. Areas where there is space for groundwater to physically rise in the aquifer can be delineated and the fixed flux boundary condition could be assigned for these locations as a comparison to the fixed head boundary condition. Such comparisons have been carried out previously, albeit not in a riparian setting, by Michael et al. (2013) and Werner and Simmons (2009), for example. Aquifer heterogeneities can be further incorporated within the SI vulnerability assessments, as their importance is noted in Vandenbohede et al. (2008) and Shalem et al. (2015). Analytic solutions to estimate the saltwater toe intruding from surface water bodies that partially penetrate the aquifer such as estuarine rivers and estuaries can be developed. Shallow groundwater salinity data (e.g., Setiawan et al., 2022a) could be further incorporated in future SI vulnerability assessments or compared against estimated vulnerabilities. Temporal variabilities of surface water and groundwater parameters (e.g., tidally fluctuating head and salinity, active and passive SI; Setiawan et al., 2023) may be considered in future SI vulnerability assessments where data is available. The SI vulnerability map outputs can also be used to highlight municipal assets such as drinking water, wastewater, and stormwater infrastructures most at–risk of groundwater salinization impacts under current and future conditions; a national gap in Aotearoa New Zealand (Setiawan et al., 2022b; Simonson & Hall, 2019). Additional methodological development is required to scale up SI vulnerability maps to regional or national scales. Aotearoa New Zealand is data–rich with numerous national–scale datasets related to hydrogeology (e.g., Westerhoff et al., 2018). Methods to validate SI vulnerability maps in the field can also be further developed.

5. Conclusions

Mapping SI vulnerability from surface water bodies hydrologically connected to the ocean is increasingly important to highlight areas for further monitoring and management, especially under future climate change and anthropogenic stresses. A new SI vulnerability tier system was created based on surface water salinity, surface water-groundwater freshwater head gradients, and the physically-based analytic solutions of Strack (1976) (developed further by Werner et al., 2012). This new SI vulnerability tier approach was applied in GIS on a city scale to assess SI vulnerability from brackish and saline surface water bodies including the ocean, estuary, and estuarine rivers under current sea level and SLR scenarios of 0.5 and 1.0 m. A fixed head inland boundary condition was applied to represent coastal cities on low–lying land with extensive drainage networks such as the study area of Ōtautahi Christchurch, Aotearoa New Zealand. The SI vulnerability tier method was compared to GALDIT–SUSI (Kazakis et al., 2019), a weighted indexing approach, for the same study area.

As the sea level rose, estuary and river levels increased, and saltwater encroachment extended further upstream in previously fresh river reaches. Stretches of the shallow unconfined aquifer adjacent to surface water bodies were categorised into SI vulnerability tiers developed in this study, based on the surface water salinity and the freshwater head difference between groundwater and surface water (symbolised as p [L]). Active SI occurs when $p < 0$ (denoting maximum SI vulnerability), while passive SI occurs when $p > 0$ (denoting moderate SI vulnerability) in the aquifer adjacent to the brackish and saline surface water bodies (i.e., > 1000 kg m^{-3} or > 1 ppt) (adapted from Werner, 2016). Where passive SI occurs, the theoretical saltwater toe position in the aquifer was calculated using the analytic solutions and mapped perpendicular to the surface water boundaries in GIS. The further inland the saltwater toe, the higher the SI vulnerability. Stretches of aquifer adjacent to fresh surface water bodies (i.e., ≤ 1000 kg m^{-3}) were considered least vulnerable to SI.

Both SI vulnerability tiers and GALDIT–SUSI agreed that SI vulnerability increased with SLR and decreased upstream of the river mouth. Based on the SI vulnerability tiers, active SI areas increased upstream along estuarine rivers and around the estuary and coastal margins under SLR. GALDIT–SUSI outputs also showed areas of the highest vulnerability around the estuary and river mouths across all sea level scenarios. Based on GALDIT–SUSI, SLR expanded high vulnerability areas further inland toward topographically low areas as elevation was considered one of the most important factors contributing to SI. GALDIT-SUSI does not consider surface water conditions in assessing SI vulnerability and lacks a hydrogeological basis in ranking and amalgamating the considered factors into one vulnerability index. Both SI vulnerability mapping methodologies and results were compared and discussed. Further research is needed to validate the SI vulnerability maps.

SI vulnerability can be assessed using physically-based methods such as the analytic solutions at a large scale in GIS, allowing for site–specific parameter combinations along kilometres of coastal, estuary, and river boundaries; an improvement over past applications of the analytic solutions to assess one cross–section per aquifer. Despite the simplicity of the SI vulnerability tiers developed, they can provide a physically-based first–pass approximation of SI vulnerability from brackish or saline surface water bodies, which can be helpful in groundwater management and decision–making processes. Alternative methods to apply the SI vulnerability tiers in a simplified approach and the analytic solutions considering a positive net recharge were provided. The SI vulnerability tiers can complement other approaches to inform groundwater managers of SI vulnerability under current and future conditions.

CRediT authorship contribution statement

Irene Setiawan: Conceptualization, Methodology, Investigation, Formal analysis, Visualization, Project administration, Writing – original draft. **Leanne K. Morgan:** Conceptualization, Methodology, Supervision, Writing – review & editing, Funding acquisition. **Crile Doscher:** Supervision, Writing – review & editing.

Declaration of competing interest

The authors declare that they have no known competing financial interests or personal relationships that could have appeared to influence the work reported in this paper.

Data availability

Data will be made available on request.

Acknowledgements

The first author was funded by the Lincoln University Doctoral Scholarship and now the New Zealand Ministry of Business Innovation and Employment (MBIE) Future Coasts Aotearoa Contract C01X2107. Leanne Morgan is supported by Canterbury Regional Council, New Zealand and the MBIE Future Coasts Aotearoa Contract C01X2107. We thank the anonymous reviewers who helped improve the manuscript. Thanks to Amandine Bosserelle for sharing the groundwater level data. Thanks to Richard Measures at NIWA for sharing the hydrodynamic model outputs and the helpful correspondence.

Appendix A. Supplementary data

Supplementary data to this article can be found online at https://doi.org/10.1016/j.jhydrol.2023.130461.

References

Barlow, P.M., Reichard, E.G., 2010. Saltwater intrusion in coastal regions of North America. Hydrgeol. J. 18 (1), 247–260. https://doi.org/10.1007/s10040-009-0514-3.

Beebe, C.R., Ferguson, G., Gleeson, T., Morgan, L.K., Werner, A.D., 2016. Application of an Analytical Solution as a Screening Tool for Sea Water Intrusion. Groundwater 54 (5), 709–718. https://doi.org/10.1111/gwat.12411.

Befus, K.M., Barnard, P.L., Hoover, D.J., Finzi Hart, J.A., Voss, C.I., 2020. Increasing threat of coastal groundwater hazards from sea-level rise in California. Nat. Clim. Chang. 10 (10), 946–952. https://doi.org/10.1038/s41558-020-0874-1.

Begg, J.G., Jones, K.E., Barrell, D.J.A., 2015. Geology and geomorphology of urban Christchurch and eastern Canterbury. Institute of Geological and Nuclear Sciences Limited, Lower Hutt, New Zealand. Retrieved from https://www.researchgate.net/profile/John-Begg/publication/312663165_Geology_and_geomorphology_of_urban_Christchurch_and_eastern_Canterbury/links/5887ac5da6fdcc6b791ec5e2/Geology-and-geomorphology-of-urban-Christchurch-and-eastern-Canterbury.pdf.

Bhattachan, A., Emanuel, R., Ardon, M., Bernhardt, E., Anderson, S., Stillwagon, M., Wright, J., 2018. Evaluating the effects of land-use change and future climate change on vulnerability of coastal landscapes to saltwater intrusion. Elem Sci Anth 6, 62. https://doi.org/10.1525/elementa.316.

Bhattachan, A., Jurjonas, M.D., Morris, P.R., Taillie, P.J., Smart, L.S., Emanuel, R.E., Seekamp, E.L., 2019. Linking residential saltwater intrusion risk perceptions to physical exposure of climate change impacts in rural coastal communities of North Carolina. Nat. Hazards 97 (3), 1277–1295. https://doi.org/10.1007/s11069-019-03706-0.

Bhuiyan, M.J.A.N., Dutta, D., 2012. Assessing impacts of sea level rise on river salinity in the Gorai river network, Bangladesh. Estuar. Coast. Shelf Sci. 96, 219–227. https://doi.org/10.1016/j.ecss.2011.11.005.

Bosserelle, A.L., Morgan, L.K., Dempsey, D.E., et al., 2023. Shallow groundwater characterisation and hydrograph classification in the coastal city of Ōtautahi/Christchurch, New Zealand. Hydrogeol J. https://doi.org/10.1007/s10040-023-02745-z.

Bosserelle, A.L., Morgan, L.K., Hughes, M.W., 2022. Groundwater rise and associated flooding in coastal settlements due to sea-level rise: a review of processes and methods. Earth's Future 10 (7), e2021EF002580. https://doi.org/10.1029/2021EF002580.

Brown, L.J., 2001. Chapter 23: Canterbury. Groundwaters of New Zealand. New Zealand Hydrological Society, Wellington, New Zealand.

Cantelon, J.A., Guimond, J.A., Robinson, C.E., Michael, H.A., Kurylyk, B.L., 2022. Vertical saltwater intrusion in coastal aquifers driven by episodic flooding: a review. Water Resour. Res. 58 (11), e2022WR032614 https://doi.org/10.1029/2022WR032614.

Christchurch City Council, 2003. Waterways, wetlands and drainage guide — Ko Te Anga Whakaora mō Ngā Arawai Rēpō. Christchurch, New Zealand. Retrieved from https://ccc.govt.nz/environment/water/water-policy-and-strategy/waterways-wetlands-and-drainage-guide.

Christchurch City Council, 2016. Ōtākaro / Avon River Catchment: Tauākī Wai Pātaua / Vision and Values. Retrieved from. https://www.ccc.govt.nz/assets/Documents/Environment/Water/Avon-River-Catchment-Vision-Values.pdf.

Christchurch City Council, 2021. Where our water comes from. Retrieved 10 March, 2021, from. https://ccc.govt.nz/services/water-and-drainage/water-supply/where-our-water-comes-from.

Controller and Auditor-General, 2020. Reflecting on our work about water management. Retrieved from. https://oag.parliament.nz/2020/water-management.

Cook, S., Dixon-Jain, P., Hocking, M., Sundaram, B., Morgan, L.K., Ivkovic, K.M., Garlapati, N., 2013. A national-scale vulnerability assessment of seawater intrusion: Vulnerability Factor Analysis (Record 2013/08): Geoscience Australia. Canberra and National Centre for Groundwater Research and Training, Adelaide. Retrieved from https://ecat.ga.gov.au/geonetwork/srv/eng/catalog.search#/metadata/74661.

Costa, Y., Martins, I., de Carvalho, G.C., Barros, F., 2023. Trends of sea-level rise effects on estuaries and estimates of future saline intrusion. Ocean Coast. Manag. 236, 106490 https://doi.org/10.1016/j.ocecoaman.2023.106490.

Cox, S.C., van Ballegooy, S., Rutter, H.K., Harte, D.S., Holden, C., Gulley, A.K., Manga, M., 2021. Can artesian groundwater and earthquake-induced aquifer leakage exacerbate the manifestation of liquefaction? Eng. Geol. 281, 105982 https://doi.org/10.1016/j.enggeo.2020.105982.

Dasgupta, S., Hossain, M.M., Huq, M., Wheeler, D., 2014. Climate change, soil salinity, and the economics of high-yield rice production in coastal Bangladesh (English). World Bank Group, Washington, DC. Retrieved from http://documents.worldbank.org/curated/en/131161468004833954/Climate-change-soil-salinity-and-the-economics-of-high-yield-rice-production-in-coastal-Bangladesh.

Dibaj, M., Javadi, A.A., Akrami, M., Ke, K.-Y., Farmani, R., Tan, Y.-C., Chen, A.S., 2021. Coupled three-dimensional modelling of groundwater-surface water interactions for management of seawater intrusion in Pingtung Plain. Taiwan. *Journal of Hydrology: Regional Studies* 36, 100850. https://doi.org/10.1016/j.ejrh.2021.100850.

Eamus, D., Fu, B., Springer, A.E., Stevens, L.E., 2016. Groundwater Dependent Ecosystems: Classification, Identification Techniques and Threats. In: Jakeman, A.J., Barreteau, O., Hunt, R.J., Rinaudo, J.-.-D., Ross, A. (Eds.), Integrated Groundwater Management: Concepts, Approaches and Challenges. Springer International Publishing, Cham, pp. 313–346. https://doi.org/10.1007/978-3-319-23576-9_13.

Esri, 2022. ArcGIS Pro (Version 3.0.1). Environmental Systems Research Institute, Redlands, CA.

Herbert, E.R., Boon, P., Burgin, A.J., Neubauer, S.C., Franklin, R.B., Ardón, M., Gell, P., 2015. A global perspective on wetland salinization: ecological consequences of a growing threat to freshwater wetlands. Ecosphere 6 (10), art206. https://doi.org/10.1890/ES14-00534.1.

Hingst, M.C., McQuiggan, R.W., Peters, C.N., He, C., Andres, A.S., Michael, H.A., 2022. Surface Water-Groundwater Connections as Pathways for Inland Salinization of Coastal Aquifers. Groundwater. https://doi.org/10.1111/gwat.13274.

Hobbs, M., Ahuriri-Driscoll, A., Kingham, S., Wiki, J., Marek, L., Dionisio, M.R., Mackenbach, J.D., 2022. A city profile of Ōtautahi Christchurch. Cities 121, 103481. https://doi.org/10.1016/j.cities.2021.103481.

Hunter, J.D., 2007. Matplotlib: A 2D Graphics Environment. Comput. Sci. Eng. 9 (3), 90–95. https://doi.org/10.5281/zenodo.4638398.

Jiao, J., Post, V., 2019. *Coastal Hydrogeology*: Cambridge University Press. https://doi.org/10.1017/9781139344142.

Kazakis, N., Busico, G., Colombani, N., Mastrocicco, M., Pavlou, A., Voudouris, K., 2019. GALDIT-SUSI a modified method to account for surface water bodies in the assessment of aquifer vulnerability to seawater intrusion. J. Environ. Manage. 235, 257–265. https://doi.org/10.1016/j.jenvman.2019.01.069.

Ketabchi, H., Mahmoodzadeh, D., Ataie-Ashtiani, B., Simmons, C.T., 2016. Sea-level rise impacts on seawater intrusion in coastal aquifers: Review and integration. J. Hydrol. 535, 235–255. https://doi.org/10.1016/j.jhydrol.2016.01.083.

Kirwan, M.L., Gedan, K.B., 2019. Sea-level driven land conversion and the formation of ghost forests. Nat. Clim. Chang. 9 (6), 450–457. https://doi.org/10.1038/s41558-019-0488-7.

Klassen, J., Allen, D.M., 2017. Assessing the risk of saltwater intrusion in coastal aquifers. J. Hydrol. 551, 730–745. https://doi.org/10.1016/j.jhydrol.2017.02.044.

Koussis, A.D., Mazi, K., Destouni, G., 2012. Analytical single-potential, sharp-interface solutions for regional seawater intrusion in sloping unconfined coastal aquifers, with pumping and recharge. J. Hydrol. 416–417, 1–11. https://doi.org/10.1016/j.jhydrol.2011.11.012.

Land Information New Zealand. (2011a, 19 February 2021). *NZ River Centrelines (Topo, 1:50k)*. Retrieved from https://data.linz.govt.nz/layer/50327-nz-river-centrelines-topo-150k/.

Land Information New Zealand. (2011b, 12 Jul 2019). *NZ River Polygons (Topo, 1:50k)*. Retrieved 9 September 2019, from https://data.linz.govt.nz/layer/50328-nz-river-polygons-topo-150k/.

Land Information New Zealand, 2021. Canterbury - Christchurch 1m DEM (2020–2021). Retrieved from. https://data.linz.govt.nz/layer/109641-canterbury-christchurch-1m-dem-2020-2021/.

Lenkopane, M., Werner, A.D., Lockington, D.A., Li, L., 2009. Influence of variable salinity conditions in a tidal creek on riparian groundwater flow and salinity dynamics. J. Hydrol. 375 (3), 536–545. https://doi.org/10.1016/j.jhydrol.2009.07.004.

Lerner, D.N., 1990. Groundwater recharge in urban areas. Atmos. Environ. Part B 24 (1), 29–33. https://doi.org/10.1016/0957-1272(90)90006-G.

Liu, T., Su, X., Prigiobbe, V., 2018. Groundwater-Sewer Interaction in Urban Coastal Areas. Water 10 (12), 1774.

Liu, Y., Zhang, C., Liu, X., Li, C., Sheuermann, A., Xin, P., Lockington, D.A., 2022. Salt transport under tide and evaporation in a subtropical wetland: field monitoring and numerical simulation. Water Resour. Res. 58 (5), e2021WR031530 https://doi.org/10.1029/2021WR031530.

Lobo-Ferreira, J. P., Chachadi, A. G., Diamantino, C., & Henriques, M. J. (2007). Assessing aquifer vulnerability to seawater intrusion using the GALDIT method: part 1 - application to the Portuguese Monte Gordo aquifer. In J. P. LoboFerreira & J. M. P. Viera (Eds.), *Water in Celtic Countries: Quantity, Quality and Climate Variability* (Vol. 310, pp. 161).

Lorenz, J.J., 2014. A Review of the Effects of Altered Hydrology and Salinity on Vertebrate Fauna and Their Habitats in Northeastern Florida Bay. Wetlands 34 (1), 189–200. https://doi.org/10.1007/s13157-013-0377-1.

Lu, C., Werner, A.D., Simmons, C.T., 2013. Threats to coastal aquifers. Nat. Clim. Chang. 3 (7), 605. https://doi.org/10.1038/nclimate1901.

Luo, C.-Y., Shen, S.-L., Han, J., Ye, G.-L., Horpibulsuk, S., 2015. Hydrogeochemical environment of aquifer groundwater in Shanghai and potential hazards to underground infrastructures. Nat. Hazards 78 (1), 753–774. https://doi.org/10.1007/s11069-015-1727-5.

Luoma, S., Okkonen, J., Korkka-Niemi, K., 2017. Comparison of the AVI, modified SINTACS and GALDIT vulnerability methods under future climate-change scenarios for a shallow low-lying coastal aquifer in southern Finland. Hydrgeol. J. 25 (1), 203–222. https://doi.org/10.1007/s10040-016-1471-2.

Macara, G.R., 2016. The Climate and Weather of Canterbury: National Institute of Water & Atmospheric Research (NIWA). Retrieved from. https://niwa.co.nz/static/web/canterbury_climatology_second_ed_niwa.pdf.

Mancini, C.P., Lollai, S., Volpi, E., Fiori, A., 2020. Flood Modeling and Groundwater Flooding in Urbanized Reclamation Areas: The Case of Rome (Italy). Water 12 (7), 2030.

Mantoglou, A., 2003. Pumping management of coastal aquifers using analytical models of saltwater intrusion [https://doi.org/10.1029/2002WR001891]. Water Resour. Res. 39 (12) https://doi.org/10.1029/2002WR001891.

Mazhar, S., Pellegrini, E., Contin, M., Bravo, C., De Nobili, M., 2022. Impacts of salinization caused by sea level rise on the biological processes of coastal soils - A review [Review]. Front. Environ. Sci. 10 https://doi.org/10.3389/fenvs.2022.909415.

Manaaki Whenua Landcare Research, 2021. LCDB v5.0 - Land Cover Database version 5.0, Mainland, New Zealand. Retrieved 3 March 2023 https://lris.scinfo.org.nz/layer/104400-lcdb-v50-land-cover-database-version-50-mainland-new-zealand/.

McKinney, W., 2010. Data structures for statistical computing in python. In: Walt, S. v. d., Millman J. (Chair), Symposium conducted at the meeting of the 9th Python in Science Conference. https://doi.org/10.25080/Majora-92bf1922-00a.

Michael, H.A., Russoniello, C.J., Byron, L.A., 2013. Global assessment of vulnerability to sea-level rise in topography-limited and recharge-limited coastal groundwater systems. Water Resour. Res. 49 (4), 2228–2240. https://doi.org/10.1002/wrcr.20213.

Moorhead, K.K., Brinson, M.M., 1995. Response of Wetlands to Rising Sea Level in the Lower Coastal Plain of North Carolina. Ecol. Appl. 5 (1), 261–271. https://doi.org/10.2307/1942068.

Morgan, L. K., Werner, A. D., Morris, M. J., & Teubner, M. D. (2013). Application of a Rapid-Assessment Method for Seawater Intrusion Vulnerability: Willunga Basin, South Australia. In C. Wetzelhuetter (Ed.), *Groundwater in the Coastal Zones of Asia-Pacific* (pp. 205-225). Dordrecht: Springer Netherlands. https://doi.org/10.1007/978-94-007-5648-9_10.

Morgan, L.K., Werner, A.D., 2015. A national inventory of seawater intrusion vulnerability for Australia. *Journal of Hydrology*. Reg. Stud. 4, Part B, 686–698. https://doi.org/10.1016/j.ejrh.2015.10.005.

Morgan, L.K., Werner, A.D., Simmons, C.T., 2012. On the interpretation of coastal aquifer water level trends and water balances: A precautionary note. J. Hydrol. 470–471, 280–288. https://doi.org/10.1016/j.jhydrol.2012.09.001.

Napolitano, P., Fabbri, A., 1996. Single-parameter sensitivity analysis for aquifer vulnerability assessment using DRASTIC and SINTACS. IAHS Publications-Series of Proceedings and Reports-Intern Assoc Hydrological Sciences 235 (235), 559–566.

National Topographic Office, 2012. NZ Coastlines and Islands Polygons (Topo 1:50k). Retrieved 25 March, 2021, from. https://data.linz.govt.nz/layer/51153-nz-coastlines-and-islands-polygons-topo-150k/.

NZ SeaRise, 2022. Maps. Retrieved from. https://www.searise.nz/maps-2.

Onodera, S.-I., Saito, M., Sawano, M., Hosono, T., Taniguchi, M., Shimada, J., Delinom, R., 2008. Effects of intensive urbanization on the intrusion of shallow groundwater into deep groundwater: Examples from Bangkok and Jakarta. Sci. Total Environ. 404 (2), 401–410. https://doi.org/10.1016/j.scitotenv.2008.08.003.

Ōpāwaho Heathcote River Network, 2021. About the River. Retrieved 16 March, 2023, from. https://ohrn.nz/about-the-river/.

Orchard, S., & Measures, R. (2016). *Development of a fine-scale salinity model for the Avon Heathcote Estuary Ihutai*: University of Canterbury and National Institute of Water & Atmospheric Research Ltd. Retrieved from https://ir.canterbury.ac.nz/handle/10092/13525.

Orchard, S., Hughey, K.F.D., Schiel, D.R., 2020. Risk factors for the conservation of saltmarsh vegetation and blue carbon revealed by earthquake-induced sea-level rise. Sci. Total Environ. 746, 141241 https://doi.org/10.1016/j.scitotenv.2020.141241.

Orchard, S., Measures, R., 2017. Sea level rise impacts in the Avon Heathcote Estuary Ihutai: Salinity intrusion and īnanga spawning scenarios [unpublished report]. Waterlink and National Institute of Water & Atmospheric Research Ltd, Christchurch, New Zealand.

Osman, O., Aina, O.D., Ahmad, F., 2017. Chemical fingerprinting of saline water intrusion into sewage lines. Water Sci. Technol. 76 (8), 2044–2050. https://doi.org/10.2166/wst.2017.374.

Parker, G.G., Ferguson, G.E., Love, S.K., 1955. Water resources of southeastern Florida, with special reference to the geology and ground water of the Miami area. U. S. Geological Survey. https://pubs.usgs.gov/wsp/1255/report.pdf.

Parsons, M., Fisher, K., Crease, R.P., 2021. Remaking Muddy Blue Spaces: Histories of Human-Wetlands Interactions in the Waipā River and the Creation of Environmental Injustices. In: Decolonising Blue Spaces in the Anthropocene: Freshwater Management in Aotearoa New Zealand. Springer International Publishing, Cham, pp. 121–179. Retrieved from doi: 10.1007/978-3-030-61071-5_4.

Passeri, D.L., Hagen, S.C., Medeiros, S.C., Bilskie, M.V., Alizad, K., Wang, D., 2015. The dynamic effects of sea level rise on low-gradient coastal landscapes: A review. Earth's Future 3 (6), 159–181. https://doi.org/10.1002/2015EF000298.

Peters, C.N., Kimsal, C., Frederiks, R.S., Paldor, A., McQuiggan, R., Michael, H.A., 2022. Groundwater pumping causes salinization of coastal streams due to baseflow depletion: Analytical framework and application to Savannah River. GA. *Journal of Hydrology* 604, 127238. https://doi.org/10.1016/j.jhydrol.2021.127238.

Pool, M., Carrera, J., 2011. A correction factor to account for mixing in Ghyben-Herzberg and critical pumping rate approximations of seawater intrusion in coastal aquifers. Water Resour. Res. 47 (5) https://doi.org/10.1029/2010WR010256.

Post, V.E.A., Banks, E., Brunke, M., 2018. Groundwater flow in the transition zone between freshwater and saltwater: a field-based study and analysis of measurement errors. Hydrgeol. J. 26 (6), 1821–1838. https://doi.org/10.1007/s10040-018-1725-2.

Prathapar, S.A., Robbins, C.W., Meyer, W.S., Jayawardane, N.S., 1992. Models for estimating capillary rise in a heavy clay soil with a saline shallow water table. Irrig. Sci. 13 (1), 1–7. https://doi.org/10.1007/BF00190238.

Renken, R.A., Dixon, J., Koehmstedt, J.A., Ishman, S., Lietz, A.C., Marella, R.L., Memberg, S., 2005. Impact of anthropogenic development on coastal ground-water hydrology in southeastern Florida, 1900–2000 (1275). Retrieved from. http://pubs.er.usgs.gov/publication/cir1275.

Riahi, K., van Vuuren, D.P., Kriegler, E., Edmonds, J., O'Neill, B.C., Fujimori, S., Tavoni, M., 2017. The Shared Socioeconomic Pathways and their energy, land use, and greenhouse gas emissions implications: An overview. Glob. Environ. Chang. 42, 153–168. https://doi.org/10.1016/j.gloenvcha.2016.05.009.

Saaty, T.L., 1990. How to make a decision: The analytic hierarchy process. Eur. J. Oper. Res. 48 (1), 9–26. https://doi.org/10.1016/0377-2217(90)90057-I.

Setiawan, I., 2018. Assessing seawater intrusion vulnerability associated with sea level rise in Christchurch, New Zealand using GIS-based methods (Honours Dissertation). Lincoln University, Lincoln, New Zealand.. Retrieved from https://researcharchive.lincoln.ac.nz/bitstream/handle/10182/10193/Setiawan_Hons.pdf?sequence=4&isAllowed=y.

Setiawan, I., Morgan, L., Doscher, C., Ng, K., Bosserelle, A., 2022a. Christchurch shallow groundwater quality survey dataset. Data Brief 41, 107982. https://doi.org/10.1016/j.dib.2022.107982.

Setiawan, I., Morgan, L., Doscher, C., Ng, K., Bosserelle, A., 2022b. Mapping shallow groundwater salinity in a coastal urban setting to assess exposure of municipal assets. J. Hydrol.: Reg. Stud. 40, 100999 https://doi.org/10.1016/j.ejrh.2022.100999.

Setiawan, I., Morgan, L.K., Doscher, C., 2023. Saltwater intrusion from an estuarine river: A field investigation. J. Hydrol. 617, 128955 https://doi.org/10.1016/j.jhydrol.2022.128955.

Shalem, Y., Weinstein, Y., Levi, E., Herut, B., Goldman, M., Yechieli, Y., 2015. The extent of aquifer salinization next to an estuarine river: an example from the eastern Mediterranean. Hydrgeol. J. 23 (1), 69–79. https://doi.org/10.1007/s10040-014-1192-3.

Shalem, Y., Yechieli, Y., Herut, B., Weinstein, Y., 2019. Aquifer response to estuarine stream dynamics. Water 11 (8), 1678. https://doi.org/10.3390/w11081678.

Shammi, M., Rahman, M.M., Bondad, S.E., Bodrud-Doza, M., 2019. Impacts of salinity intrusion in community health: a review of experiences on drinking water sodium from coastal areas of bangladesh. Healthcare 7 (1). https://doi.org/10.3390/healthcare7010050.

Shen, C., Jin, G., Xin, P., Kong, J., Li, L., 2015. Effects of salinity variations on pore water flow in salt marshes. Water Resour. Res. 51 (6), 4301–4319. https://doi.org/10.1002/2015WR016911.

Simonson, T., Hall, G., 2019. Vulnerable: the quantum of local government infrastructure exposed to sea level rise. Local Government in New Zealand, Wellington, New Zealand. Retrieved from https://www.lgnz.co.nz/our-work/publications/vulnerable-the-quantum-of-local-government-infrastructure-exposed-to-sea-level-rise/.

Stats NZ, 2022. *Subnational population estimates: At 30 June 2022 (provisional)*. Retrieved 23 December, 2022, from https://www.stats.govt.nz/information-releases/subnational-population-estimates-at-30-june-2022-provisional/.

Stewart, M.K., 2012. A 40-year record of carbon-14 and tritium in the Christchurch groundwater system, New Zealand: Dating of young samples with carbon-14. J. Hydrol. 430–431, 50–68. https://doi.org/10.1016/j.jhydrol.2012.01.046.

Stewart, M.K., Morgenstern, U., Tsujimura, M., Gusyev, M.A., Sakakibara, K., Imaizumi, Y., Cox, S.C., 2018. Mean residence times and sources of Christchurch springs. Journal of Hydrology (new Zealand) 57 (2), 81–94. https://www.jstor.org/stable/26643851.

Strack, O.D.L., 1976. A single-potential solution for regional interface problems in coastal aquifers. Water Resour. Res. 12 (6), 1165–1174. https://doi.org/10.1029/WR012i006p01165.

Tully, K., Gedan, K., Epanchin-Niell, R., Strong, A., Bernhardt, E.S., BenDor, T., Weston, N.B., 2019. The Invisible Flood: The Chemistry, Ecology, and Social Implications of Coastal Saltwater Intrusion. Bioscience 69 (5), 368–378. https://doi.org/10.1093/biosci/biz027.

Vandenbohede, A., Lebbe, L., Gysens, S., Delecluyse, K., DeWolf, P., 2008. Salt water infiltration in two artificial sea inlets in the Belgian dune area. J. Hydrol. 360 (1), 77–86. https://doi.org/10.1016/j.jhydrol.2008.07.018.

Webster, I.T., Norquay, S.J., Ross, F.C., Wooding, R.A., 1996. Solute exchange by convection within estuarine sediments. Estuar. Coast. Shelf Sci. 42 (2), 171–183. https://doi.org/10.1006/ecss.1996.0013.

Weissman, D.S., Tully, K.L., 2020. Saltwater intrusion affects nutrient concentrations in soil porewater and surface waters of coastal habitats. Ecosphere 11 (2), e03041.

Werner, A.D., Ward, J.D., Morgan, L.K., Simmons, C.T., Robinson, N.I., Teubner, M.D., 2012. Vulnerability Indicators of Sea Water Intrusion. Ground Water 50 (1), 48–58. https://doi.org/10.1111/j.1745-6584.2011.00817.x.

Werner, A., 2016. On the classification of seawater intrusion. J. Hydrol. 551 https://doi.org/10.1016/j.jhydrol.2016.12.012.

Werner, A.D., Bakker, M., Post, V.E.A., Vandenbohede, A., Lu, C., Ataie-Ashtiani, B., Barry, D.A., 2013. Seawater intrusion processes, investigation and management: recent advances and future challenges. Adv. Water Resour. 51, 3–26. https://doi.org/10.1016/j.advwatres.2012.03.004.

Werner, A.D., Lockington, D.A., 2006. Tidal impacts on riparian salinities near estuaries. J. Hydrol. 328 (3), 511–522. https://doi.org/10.1016/j.jhydrol.2005.12.011.

Werner, A.D., Simmons, C.T., 2009. Impact of sea-level rise on sea water intrusion in coastal aquifers. Groundwater 47 (2), 197–204. https://doi.org/10.1111/j.1745-6584.2008.00535.x.

Westerhoff, R., White, P., Miguez-Macho, G., 2018. Application of an improved global-scale groundwater model for water table estimation across New Zealand. Hydrol. Earth Syst. Sci. 22 (12), 6449–6472. https://doi.org/10.5194/hess-22-6449-2018.

White, E., Kaplan, D., 2017. Restore or retreat? saltwater intrusion and water management in coastal wetlands. Ecosyst. Health Sustainability 3 (1), e01258.

Wilson, J., 1989. Christchurch - Swamp to City - A Short History of the Christchurch Drainage Board 1875–1989. Te Waihora Press, Lincoln, New Zealand. Retrieved from https://canterbury.royalcommission.govt.nz/documents-by-key/20110929.37.

Worland, S.C., Hornberger, G.M., Goodbred, S.L., 2015. Source, transport, and evolution of saline groundwater in a shallow Holocene aquifer on the tidal deltaplain of southwest Bangladesh. Water Resour. Res. 51 (7), 5791–5805. https://doi.org/10.1002/2014WR016262.

Wriedt, G., Bouraoui, F., 2009. Large scale screening of seawater intrusion risk in Europe : methodological development and pilot application along the Spanish Mediterranean coast: Joint Research Centre. Institute for Environment Sustainability. Https://www. https://doi.org/10.2788/19371.

Xin, P., Wilson, A., Shen, C., Ge, Z., Moffett, K.B., Santos, I.R., Barry, D.A., 2022. Surface water and groundwater interactions in salt marshes and their impact on plant ecology and coastal biogeochemistry. Rev. Geophys. 60 (1), e2021RG000740 https://doi.org/10.1029/2021RG000740.